Master Erasmus Mundus in

Color in Informatics and Media Technology (CIMET)

Mobile Phone Camera Possibilities for Spectral Imaging

Master Thesis Report

Catalin Matasaru

Academic Supervisors: Prof. Markku HAUTA-KASARI (UEF)

CTO Petri PIIRAINEN (SoftColor Oy Ltd)

Jury Committee:

Defended at the University of Eastern Finland, Joensuu, Finland

June, 13, 2014

Mobile Phone Camera Possibilities for Spectral Imaging

Catalin Matasaru

June 2014

Abstract

In the past years, we have witnessed the development of a new era, a technology driven digital era. One product of this new era is considered to be the smart-phone. It incorporates a lot of devices that were once heavy, bulky, and expensive, all into a single medium. The smart-phone has become widely available for every user and is nowadays a part of our daily life.

One special device that the smart-phone incorporates is the digital camera. In the beginning the embedded mobile cameras were of poor quality and were considered a poor choice to the unmatched high end digital cameras. However in recent years developments have been made in the newer generation sensors which are more accurate, widely available and inexpensive. Technology trends shows that the new sensor generations continue pixel size reduction and promising new technologies are added such as back-side illumination and organic film materials [87]. The new generations of mobile phone cameras are closing fast the big gap that has existed so far between the professional digital single-lens reflex (DSLR) cameras and the 'simple' mobile cameras. This stems the idea that particular applications that once used the high end DSLR cameras can now be made available for mobile cameras; and even more, now giving the possibility that computations that were once necessary to be made on a separate medium, now to be made on the mobile device itself. One such application is the usage of the output of the mobile camera that through estimation algorithms to be able to recover the spectral reflectance information.

The thesis is focused in studying the practicality and usefulness of the information obtained as output from the smart-phone RGB camera (in the JPEG data type) in spectral imaging as it will be used to provide a basis in future applications where spectral data is needed such as mobile imaging in artworks, cultural heritage, medical analysis, pattern recognition (automated photo editing), etc. The study in the thesis is structured as a comparison between smart-phone cameras and DSLR cameras as their digital output in the form of RAW (obtained mainly from the DSLR cameras) and JPEG type data provides an important role in obtaining the spectral estimation of the imaged objects. Steps in creating the JPEG type image such as compression and image processing algorithms are studied to see their importance in retrieving the estimation of the spectral data.

For test purposes seven devices have been used: two digital single lens reflex (DSLR) cameras that allowed capturing the raw data, one commercial digital camera and four current smart-phone cameras. Also one of the smart phone cameras allowed capturing the raw data which was also used in tests. The methods used for estimation were linear fitting via least squares, and multivariate polynomial fitting via least squares (the second and third degree polynomials were used). In order to evaluate the performance of the reflectance recovery of the selected estimation models different metrics were used. To evaluate spectrally the differences, the methods used were: root mean square error (RMSE), goodness of fit coefficient (GFC) and also RMSE wavelength-wise. Also to evaluate colorimetrically the performance of the reflectance estimation the CIELAB and CIEDE2000 color difference metrics were used.

Preface

This thesis was submitted for the Degree of Master of Science in Color in Informatics and Media Technology (CIMET). It was financed by the European Union under the Erasmus Mundus scholarship. The work presented in this thesis has been carried out under the aegis of SoftColor Oy Company at the Spectral Color Research group in the School of Computing Department of the University of Eastern Finland, Finland, between January 2014 and June 2014.

Through my endeavors I encountered many great people, who have left an imprint in my work and also in me as person to which I am forever indebted and thankful.

I am deeply grateful to my supervisor's professor Markku Hauta-Kasari and Petri Pirainen from SoftColor Company. I am immensely grateful to professor Hauta-Kasari for his counseling, supervision and care from the beginning of my thesis up to the end. His valor, optimism, cheerfulness, vibrant nature and logical guidance have been an inspiration and enabled me to take the correct steps in developing and completing my research successfully. Of equal importance to me was the guidance, instruction and help I received from Petri Pirainen. His fortitude and enthusiastic nature coupled with his feedback, constructive comments and fruitful discussions from the many meetings were invaluable to me in constructing and finishing my work.

I would like to express my gratitude to Dr. Ville Heikkinen for his advice, valuable discussions and comments on my work. Also M.Sc Arash Mirhashemi has my sincere gratitude for all his help and fruitful dialogues made throughout the development of my project. Productive feedback from M.Sc Ana Gebejes, were also very useful to me, for which I offer many thanks.

Also I offer my grateful appreciation to all the people who gave me their precious time and helped me in all forms regarding the laboratory work. I make a special reference here for M.Sc. Piotr Bartczak, M.Sc. Tapani Hirvonen, M.Sc. Niko Penttinen and Dr. Joni Orava, all to whom I am highly indebted.

Furthermore I would like to thank my CIMET colleagues Clara Camara, Gboluwaga Oguntona, M.Sc. Nina Rogelj and Yingfei Xiao for providing me with ideas and much needed support in times of crisis.

Even more I would like to thank my family and all my friends for providing me with much needed moral support.

Last but not least I would to express my gratefulness and love for my SO Andreea who was always the main pillar of moral support, encouragement and love throughout my CIMET master.

Joensuu, June 2014

Catalin Matasaru

Contents

List of Figures

List of Tables

1 Introduction

1.1 Background

In the recent years there has been a huge development on the mobile phone market in terms of technology, especially the smart-phone market [1]. This has led in turn to a large consumerism market, making smart-phones and their technology widely available for every user, and becoming nowadays a part of our daily life.

The confluence of the phone camera and the mobile device has been highly attractive since its inception. Combining the telecommunications connectivity and the proper medium for photography has proven to be highly popular in the history of mobility and the history of photography. Due to this, mobile cameras cannot be considered as any other type of cameras, instead "*camera phones are extending personal imaging practices and allowing for the evolution of new kinds of imaging practices*". [2, 3] This statement is particularly true considering all the advances that have been made in the new generation sensors which are more accurate, widely available and inexpensive. Technology trends shows that the new sensor generations continue pixel size reduction and promising new technologies are added such as back-side illumination and organic film materials[87]. The new generations of mobile phone cameras are closing fast the big gap that has existed so far between the professional digital single-lens reflex (DSLR) cameras and the 'simple' mobile cameras. This stems the idea that particular applications that once used the high end DSLR cameras can now be made available for mobile cameras; and even more, now giving the possibility that computations that were once necessary to be made on a separate medium, now to be made on the mobile device itself, as current devices come with low-power high-performance processors.

Figure 1 Interaction of light and object in order to obtain the phone camera color signal

In this context mobile devices can be exploited further by utilizing their full hardware and software potential. An application to be studied would be the usage of the phone camera as a capturing device and through further estimation algorithms to be able to recover the spectral information. Spectral reflectance represents physical information

of an object surface [4]. Literature provides a myriad of possibilities in the recovery of spectral reflectance. These include: liquid crystal tunable filters (LCTF) coupled with a monochrome camera [5], a six-position filter wheel containing absorption filters couple with a monochrome camera, and a two-position filter slider containing absorption filters coupled with a color-filter array (CFA) color camera [6], direct sight spectrograph [7], or dichroic mirrors devices [8]. Said devices can provide indeed accurate results, but also have some drawbacks such as high costs, high-level of expertise needed to utilize them, and they may require extra hardware for imaging which can become problematic in some types of environments. Compared to the above mentioned devices the smart-phone cameras provide an inexpensive, fast, practical and widely available solution.

Object information, when captured by a phone camera is captured in terms of a color signal, which is a product of the object spectral reflectance and the illuminant, as shown in Figure1. Therefore the cameras output is illuminant dependent. An increase of applications in many different fields requires the objects true spectral reflectance information which is independent on the viewing illuminant, hence the importance of providing the spectral information from the cameras RGB response values. So far applications tested on high end DSLR cameras provide good results in terms of reflectance estimation which leads to believe that the the new sensor technologies in current smart-phone cameras will also provide good results. Examples of fields where DSLR cameras give good results and can also be extended to smart-phone cameras include: fruit identification and quality control, material classification [10], artwork imaging [11, 14], printing industry [12], medical imaging [13], or distinguishing between metameric pairs [10]. A pair is called metameric if they match in color under the same type of illuminant, but if the illuminant is changed the match in color doesn't hold true anymore, due to the different spectral reflectance that the pairs have[16]. An example of usage for smartphones in distinguishing metamerism might be in the leather industry: a customer wants to buy a leather jacket and matching pair of shoes. The items might look color-wise the same in the shop, but under a different environment where the illuminant is changed the items will look different. In such a case we see the importance of having spectral information of the objects so we can ascertain if the color of jacket and the shoe are the same. The smart-phone through its camera and processing system can be used to obtain an estimate of the spectral reflectance and thus a solution to the problem. This allows spectral imaging in the pocket of every user of mobile devices.

1.2 Research Objective

RGB camera devices are generally considered metameric imaging devices, in opposition to spectral imaging which uses a high number of spectral channels, ranging from values higher than there to several hundred, depending on the applications [17]. Metameric imaging is considered in respect to the human visual system (HVS). The HVS uses its three types of cone receptors to process the spectral data over the visible (VIS) wavelength range of 380-780 nm in order to produce a three-channel color image. This image is considered metameric because, independent on the type of the illuminant, the same color response is produced in the three integrated channels. The same can said about a color RGB camera where we obtain the same image color output from a variety of illuminants [17]. Because of this we can

assert that the RGB camera was not built with the idea of recovering spectral information but rather for obtaining an image that is visually pleasant for the observer [18]. Furthermore due to a short number of spectral bands with broad bandwidth and the need for aprioric data information, RGB devices are not perfectly suitable for measuring spectral information. However due to the rapid development of new technologies in color cameras and also a broad number of reflectance estimation techniques, the RGB devices provide a practical, inexpensive and fast solution in recovering spectral information.

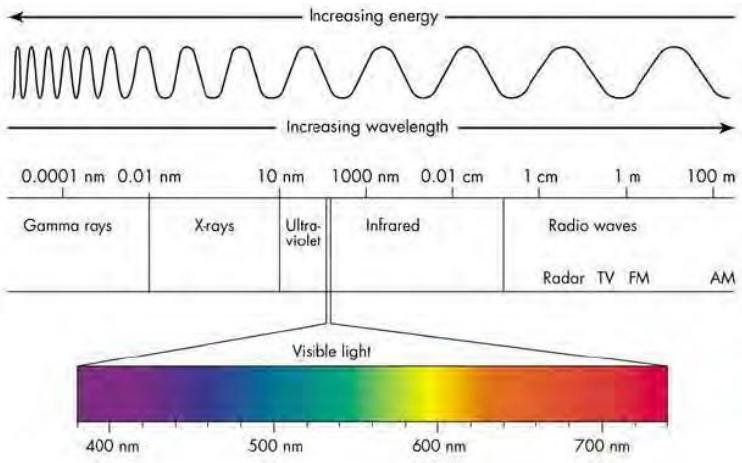

Figure 2 Electromagnetic Spectrum [19]

In the field of spectral imaging and color engineering many reflectance estimation models have been introduced. These models usually use the "raw" camera output data from the DSLR cameras, which is the direct sensor response and has not been subjected to any processing type. This approach provides good results, as seen in [10-14]. In most cases though, the digital output of the mobile camera is not a raw file but rather is stored as JPEG or TIFF data files, and each channel of the red, green, blue is obtained through an image processing engine. This type of data is quite different from the raw, unaltered data, as it suffers from many post-processing steps such as: white balance, color interpolation, color correction, gamma correction, color space conversion, saturation enhancement, compression, etc. [21-24]. Figure 3 provides a clear view of the digital camera signal processing pipeline and the most common steps required in obtaining the digital image. Few studies have considered the current mobile BSI camera sensors and its JPEG output files and studied its utility in terms of spectral recovery. There is however studies showing use of previous generation of mobile cameras [15, 25, 10, 82-86].

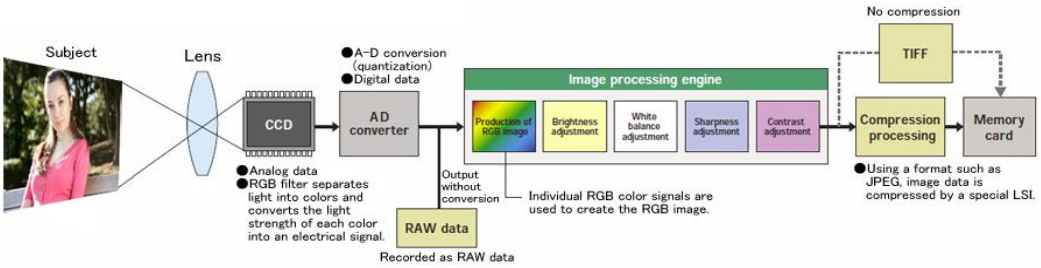

Figure 3 Digital camera signal processing pipeline [20]

Questions are raised concerning how the steps involved in the making of a digital image affect reflectance estimation models. For this, four smart-phone cameras, two DSLR cameras and one simple commercial digital camera were used for testing. The estimation methods employed were: linear fitting via least square (also known as the pseudo-inverse method [26, 27, 29, 30, 31 and 32], or simply as linear Wiener estimation method [14]) and an improvement of the first by using multivariate polynomial fitting via least squares [28, 32].

Further related questions:

Question 1: Why do we choose a professional DSLR instead of a simple mobile phone camera, or a simple daily usage camera, in terms of reflectance estimation?

Question 2: What type of reflectance estimation models can be used?

Question 3: Are the image processing steps important factors?

Question 4: Is the level of compression an important factor?

Question 5: Spectral imaging in your pocket?

By answering these questions the thesis intends to provide a study in the practicality and usefulness of the information obtained as output from the smart-phone RGB camera compared to the raw data information used from DSLR cameras in terms of spectral imaging estimates and it will be used to provide a basis in future applications such mobile imaging in artworks, cultural heritage, medical imaging, etc.

1.3 Outline and Contents of the thesis

The thesis is structured in six chapters, including the introduction chapter. Chapters two and three include literature review and theoretical backgrounds. Chapter two reviews the mechanism of how the human vision works and its importance to conventional imaging. Also discussed are sensors in digital cameras with focus on the current sensors in smartphones. Spectral imaging and its importance is also presented in this chapter. Chapter three describes spectral estimation techniques such as Wiener estimation method, liniar estimation method and multivariate polynomial method via least squares. Also different spectral metrics are discussed. Furthermore JPEG compression algorithm is also presented. Chapter four presents data

acquisition devices, acquisition setups employed in the current work also data preprocessing methods. Chapter five presents the main results of the work and also discussion upon the results is ensured. The final chapter of the thesis is Chapter six where conclusions are drawn and future work is presented.

2. Literature Review

2.1 Human Vision

In this chapter mechanism of the human eye and visual perception are presented as the human vision system is considered a base for conventional imaging.

Light is radiation in the form of electromagnetic waves that make vision possible to the human eye. Human eye is sensitive only to a narrow band of the electromagnetic spectrum, the visible spectrum having the spectral range between 380 to 780 nm [67].

Structure of the human eye is presented in Figure 4. Human eye is of a sphere like shape of about 24 mm in diameter. The corresponding components are cornea, aqueous humor, iris, pupil, lens, vitreous humor, retina and optic nerve. Incoming light falls onto the cornea, which is then partially refracted before reaching the lens. The quantity of light that reaches further on is restrained by the iris. The lens has the role of focusing the image. Once the light has passed it reaches then the retina. The retina contains two types of light sensitive cells, the rods and the cones. The rods perceive brightness or darkness in relatively dark environments, and cones perceive color in relatively bright environments. The names 'rods' and 'cones' are derived from the shapes of the cells. There are three types of cone cells, present in the ratio of about 32:16:1, which responds to long-, medium- and short-wavelength light, respectively. [67]. Attached to the light sensitive cells are nerve endings, which are named collectively the optic nerve. This passes the information collected at this point to the brain for interpretation.

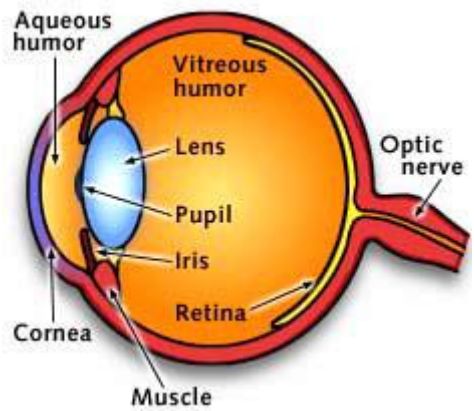

Figure 4 Structure of human eye [68]

The human eye can see an object in direct sunlight or at night without moonlight. In order to be able to accustom the eye over such a wide range of illuminance, the pupil

adjusts the quantity of light reaching the retina by varying its size. Thus the change in pupil diameter is insufficient for full control of the quantity of light. Accordingly, the rods and cones share the function by changing the responsivity of the retina. In a relatively bright environment, the cones alone function to give what is called photopic vision. In a relatively dark environment, the rods alone function to realize what is called scotopic vision. In environments having an intermediate brightness between photopic vision and scotopic vision, both the cones and the rods function to provide what is called mesopic vision [67, 69, 70].

In human vision system the colors are sensed by three types of cones named L, M, S. The cones are maximally sensitive to long (red type of light), medium (green type of light) or short (blue type of light) wavelengths of light [72]. The wavelength response curves of the LMS are shown in Figure 5.

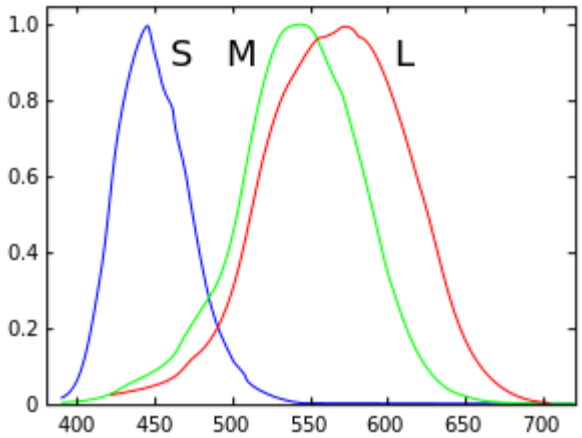

Figure 5 Long, Medium and Short cone responses [71]

Responses of the cones can be precisely modeled by a linear system defined as the spectral sensitivities of the cones, under a fixed set of viewing conditions [73]. If spectral power distribution of incident light is given by function $f(\lambda)$, the linear model containing the cone responses is given by the following equation:

$$c = \int_{\lambda_{\min}}^{\lambda_{\max}} S_i(\lambda) f(\lambda) d\lambda \qquad i \in \{1,2,3\} \tag{2.1}$$

, where $S_i(\lambda)$ represents the spectral sensitivity function of the ith type cone, $\lambda_{\min}, \lambda_{\max}$ represent the minimum and maximum wavelength.

If N uniform wavelengths are sampled over the visible region range then the model will be:

$$c = \int_{i=1}^{N} S_i(\lambda_i) f(\lambda_i) d\lambda$$
$$i \in \{1, 2, 3\} \qquad (2.2)$$

, where λ_i is the uniformly spaced wavelength.

2.2 Digital Camera Sensors

The process of creating a digital image is very similar to that of human visual system in that both respond to light and in particular images. Thus light, reflected from an object, enters the camera and passes through a set of lens. The lens focuses the light into a set of sensor and filter (such as the Bayer filter), after which the light is recorded electronically. Therefore in the process of creating a digital image the sensor plays an important role.

This chapter presents operating principles of two of the most used sensor type in digital cameras namely: CCD and CMOS image sensors. Also focus in this chapter is given to BSI type sensors as they represent presently the most used sensors in today's smartphone cameras. [57-60]

2.2.1 CCD sensor

The Charged Coupled Device (CCD) was invented in 1970 by Willard Boyle and George Smith at Bell Laboratories, USA [64].

A CCD is an electrical device that is used to create images of objects, store information (analogous to the way a computer stores information), or transfer electrical charge (as part of larger device). It receives as input light from an object or an electrical charge. The CCD takes this optical or electronic input and converts it into an electronic signal - the output. The electronic signal is then processed by some other equipment and/or software to either produce an image or to give the user valuable information [63].

CCDs are integrated circuits (ICs), that allow light to fall on the silicon chip (or die) a small glass window is inserted in front of the chip. Conventional ICs are usually encapsulated in a black plastic body to primarily provide mechanical strength, but this also shields them from light, which can affect their normal operation. CCDs are manufactured using metal-oxide-semiconductor (MOS) fabrication techniques, and each pixel can be thought of as a MOS capacitor that converts photons (light) into electrical charge, and stores the charge prior to readout [64].

Each pixel that makes up a CCD is essentially a MOS capacitor. There are usually two types of MOS capacitors: surface channel and buried channel. The two differ only slightly in their fabrication. However buried channel capacitors offer major advantages, and because of this, nearly all CCDs manufactured today use this preferred structure. A schematic cross section of a buried channel capacitor is shown in Figure 6. The device is typically built on a p-type silicon substrate with an n-type layer formed on the surface. A thin silicon dioxide layer is grown followed by a metal

electrode (or gate). The application of a positive voltage to the electrode reverse biases the p-n junction and this causes a potential well to form in the n-type silicon directly below the electrode. Incident light generates electron-hole pairs in the depletion region, and due to the applied voltage, the electrons migrate upwards into the n-type silicon layer and are trapped in the potential well. The buildup of negative charge is thus directly proportional to the level of incident light. Once the exposure time has elapsed, the charge trapped in the potential well is transferred out of the CCD before being converted to an equivalent digital value [65].

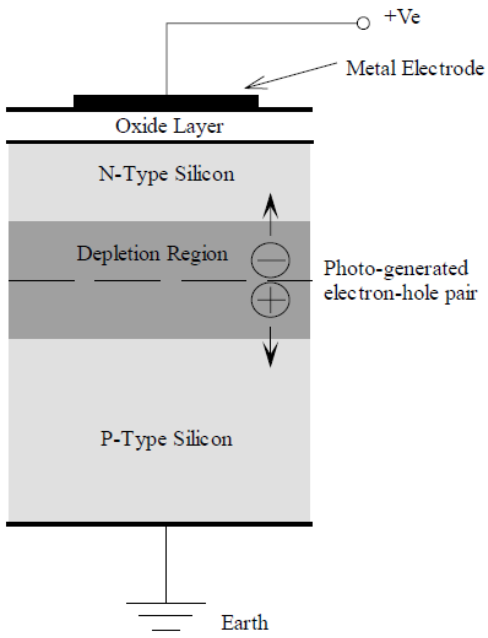

Figure 6 Burried channel capacitor CCD pixel [65]

2.2.2 CMOS sensor

Complementary metal oxide semiconductor or (CMOS) are another type of image sensors used in digital cameras. They first appeared in 1993 through the work of Jet Propulsion Laboratory (JPL) which produced a CMOS sensor with a performance comparable to scientific-grade CCDs [66].

Similar to CCDs , CMOS sensors are also comprised of light sensitive elements, which, like CCDs, are formed from a grid of light sensitive elements, each capable of producing an electrical signal/charge proportional to the incident light. However, the process of achieving this is very different in the CMOS sensor compared to the CCD sensor type. Previously we noticed that, a CCD pixel is formed from a biased p-n junction that creates a potential well in which charge accumulates during the integration period. CMOS pixel makes use of a photodiode, a capacitor and up to three transistors. Prior to the start of the integration period, the capacitor will be charged to some known voltage. When the integration period begins, the charge on the capacitor is allowed to slowly drain away through the photodiode, the rate of drain

being directly proportional to the level of incident light. At the end of the integration period, the charge remaining in the capacitor is read out and digitized [65].

Figure 7 shows an example of an active pixel and also graphs of voltage vs. time taken from various points within the pixel [65].

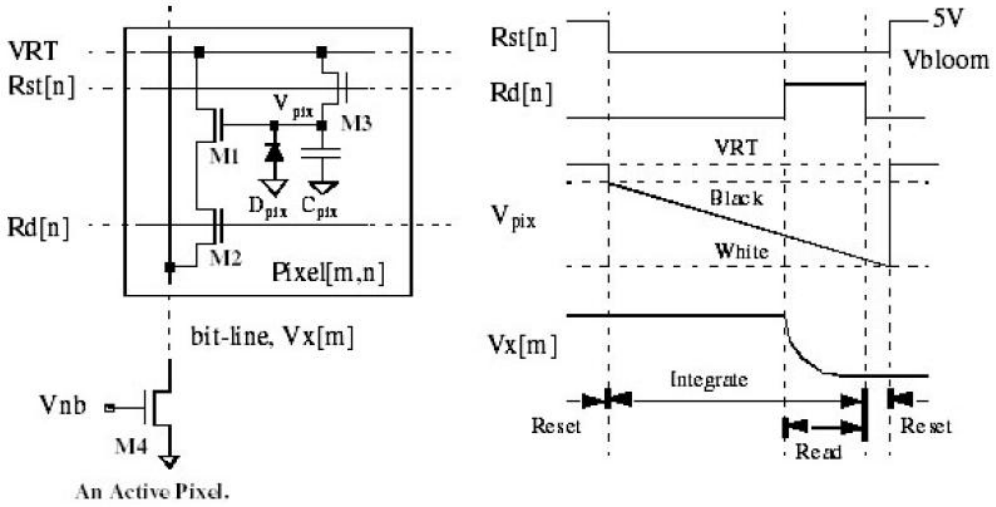

Figure 7 Active CMOS pixel structure [65]

2.2.3 BSI sensors

Demand for improved resolution in imaging systems has grown in fields such as machine vision and industrial imaging industries.

Until recently, because of the way chips are manufactured, most camera sensors have captured light at the bottom, from underneath layers of interconnections. The reason for this was the lower costs associated with their high-volume manufacturing compatibility. Manufacturers were compelled to reduce the pixel size, in order to keep cost constraints to a minimum, thus limiting the performance of image sensors. This is the main reason why the early market in smartphone cameras included mainly front illuminated sensors [57].

The recent introduction of Back-Illuminated Sensors (BSI) has made it possible to build sensors with the photo-receptive facing the light. The main advertised advantage is increased low-light performance. This technology has shown promise regarding the improvement of digital photos and video on consumer goods ranging from basic cameras to SLRs [59].

The main idea behind these new sensors is that they eliminate the light blocked by the electronic parts in order to improve the clarity of the image. Sony and Nikon have been backing BSI technology since 2009 by including the Exmor R back-illuminated CMOS sensor in several of their products [58].

Presently, the structure of the image sensors is similar in structure with human and most animal eyes in the way that the photosensitive part is on the side furthest away from the light. This makes it easier to provide circulation to the energy-hungry rods and cones cells found in biological eyes while permitting easy removal of debris from the organ [60]. In the case of artificial sensors silicon is used for both the chip and the transformation of photons into electrical energy. It is therefore easy to create the photosensitive areas in the substrate silicon and stack the electronics on top while leaving openings in the wiring over each photosite (pixel) to allow light to pass through. However, as camera resolutions have increased, pixel sizes have decreased resulting in more and more of the surface area of the sensor being covered by wiring, resulting in less and less light reaching the photosites [60]. This lead to a need to find a way to move the photosensitive region to the top of the chip, allowing it to gather more light. Optimized back-illuminated sensors can extend the spectral range down to deep-UV levels while maintaining high and stable responsivity. They also improve the system's performance by capturing more light, which improves the signal-to-noise ratio, increases the inspection speed and minimizes damaging UV exposure to delicate semiconductor devices.

As stated above, the main issue with current sensors is that a pixel is a lot more than just the photodiode as it also includes transistors and wiring for amplifying the charge, transferring it to the signal processing portion of the chip, and resetting itself between frames (Figure 8). Those electronics get placed on top of the silicon layer, partially obscuring it from the light and resulting in a well-like appearance for a typical pixel [61].

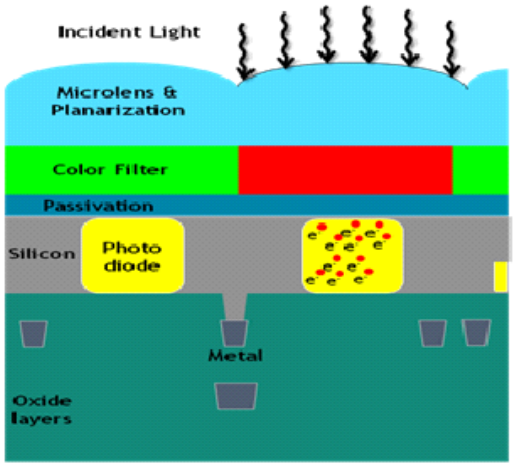

Figure 8 Simplified diagram of a backside iluminated (BSI) pixel[61]

This naturally results in a reduced amount of light due to bouncing off the wiring and penetration angle. Typical sensor fill factors — the portion of light successfully captured — range from 30% to 80%. By contrast, a back-illuminated sensor can have a fill factor of nearly 100%. Light bouncing inside electronics can also cause other problems such as vignetting and cross-talk. Thus a design which puts the photodiodes on top is clearly desirable. Having the photosensitive area on the side of the chip facing the light also dramatically improves the angular response of the sensor [60].

The main difficulty in manufacturing sensors with the photo receptors on top comes from the fabrication process. In order to have a silicon layer on top of it is necessary to build a chip the same way as a traditional front-illuminated and then place another layer of silicon substrate on top and flip the entire silicon sandwich over. After that, the original silicon base, now on top, has to be thinned to make it act as a light-sensitive layer. In order to achieve this, the back layer of a BI sensor has to be between 5-10 microns thick (less than 1% of the original thickness). Given that the wafer-thinning operation is performed as the last step, any yield loss significantly affects cost. Because the BSI wafer has been inverted, the incident light in BSI first strikes the silicon volume away from the photodiode where light may be lost from crosstalk due to diffusion to adjoining pixels or lost due to diffusion and recombination at the back interface. Blue light in particular is susceptible to this phenomenon, resulting in decreased blue QE and increased crosstalk. These issues can be addressed with the introduction of a deeper photodiode to capture the blue light and through advanced backside processing [61].

Starting with a carefully engineered silicon-on-insulator substrate, the buried oxide layer is used as a natural etch-stop to allow the ultrathin silicon to be used as a precisely controlled light collection region. This approach simplifies manufacturing significantly, improves uniformity and substantially reduces cost. Also, it allows easier scalability for wafers up to 300 mm in diameter [57].

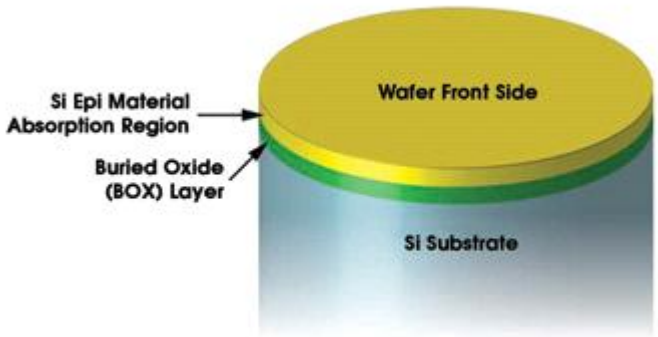

Figure 9 Cross section of a ultrathin silicion-on-insulator wafer [57]

Choosing the proper buried oxide thickness can provide the desired antireflection coating. Use of a silicon-on-insulator substrate allows room for innovative designs as well, which can offer many other benefits, including lower power and better parasitic (Figure 9). However, with most of the barriers mostly solved, it is estimated that 75% of the smartphones shipped in 2014 will come with BSI sensors [57].

Future directions in this technology go towards stacking several chips in order to create A sensors. This design would allow for a better optimization of the sensor's structure: the top chips can be used for capturing the light and those underneath can do the signal processing. Sony has already started sampling a stacked version of a BI sensor called Exmor RS. Olympus has also demonstrated how a stacked architecture

can create new possibilities. The Olympus design transfers all of the charge off the sensor at once, to the lower, shielded layer, where they can then be read out accurately [60].

2.3 Spectral imaging

Spectral imaging is a technology that provides images at multiple wavelengths and hence generates precise optical spectra at every pixel. Spectral imaging is a growing field, made possible through the new developments in technology such as in new detectors, optics, and spectral imaging techniques. A variety of technologies are now available for use and spectral imaging is a well established technique. [80]

A great deal of attention is given to spectral imaging lately and this is due to the numerous applications areas where spectral information is needed. The primary application for spectral imaging was in the area of remote sensing and terrestrial military. Nowadays however spectral imaging is used in different type of domains such environmental monitoring, material analysis, computer vision and industrial quality control. Also spectral information was used in medical imaging such as to analyze skin color, to simulate adaptation in the human vision system or to improve color reproduction of electronic endoscopes. Furthermore we see spectral imaging used in cultural heritage as it is a noninvasive type of approach [81].

2.3.1 Spectral Imaging Devices

There are different approaches for obtaining spectral images. One approach acquires a sequence of images at different wavelengths. This can be implemented by using multiple-position filter wheel containing absorption filters coupled with a monochrome camera [6]. Another approach captures the spectrum by scanning line the line the imaged object, where each line contains the complete spectrum. This type of implementation requires an imaging spectrograph coupled to a monochrome camera. The whole spectral imaged is obtained after the object is scanned completely either by moving the object or either by moving the spectral device in small increments. [7]

Other approaches include liquid crystal tunable filters (LCTF) coupled with a monochrome camera which uses electronically controlled liquid crystal elements to select and transmitted wavelength range of interest while blocking all others [5].

Even more another approach in retrieving the spectral image can be the usage of acousto-optical tunable filter (AOTF) is an electronic dispersive device based on the principle of interaction between an ordinary ray (o-ray), an extraordinary ray (e-ray), and a traveling acoustic wave in a birefringent crystal [5]

2.3.2 Structure of Spectral Image

Normal spectral imaging color is captured by using three primary colors. Color in a digital camera is captured through a color filter array (CFA). Conventional CFA is represented by a three color Bayer filter, where each color is formed through red, green and blue filters [53, 54].

In the case of spectral imaging, each pixel contains a color spectrum with tens, or hundreds of color channels. When considering the case of normal digital images, the spectral image contains information from the visible part of the spectrum, ranging from the 400-700nm range.

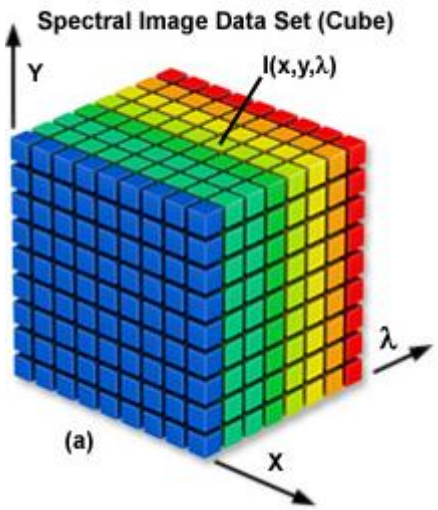

Figure 10 Structure of a spectral image [62]

The RGB image contains three gray scale channel images which are acquired through three filters. The spectral image however contains multiple gray scale channel images, which can be visualized in the form of a "data-cube", where each gray scale image represents spatial information at a specific wavelength (Figure 13). Hence when the spectral image is captured by considering the visible spectral range from the 400 to 700 nm region by 10 nm steps, the image consists of 31 different gray scale channel images.

3. Methodology

3.1 Spectral Estimation Methods

Literature has provided many kinds of spectral estimation methods in order to reproduce the spectra from three-band or from multispectral images. A small classification divides these methods into two categories [26] or three categories [27], where the pseudo-inverse model is considered as the third category. The first two categories include: Wiener estimation model, which minimizes the mean square errors (MSEs) between the real measured spectral reflectance and the estimated reflectance spectra, and the second is the finite-dimensional linear model, where the spectral reflectance is represented as linear combination of ortho-normal basis vectors.

Wiener estimation model requires three matrixes: the autocorrelation matrix of spectral reflectance, the spectral sensitivity of the camera sensor and the system noise, in order to recover the spectral reflectance. The system noise and the autocorrelation matrix represent a crucial point in characterizing the efficiency of the estimation as seen in [34].

The finite-dimensional linear model takes advantage of the representation of the linear model, where the spectral reflectance is represented as a weighted sum of a set of basis functions, which can be obtained by applying principal component analysis (PCA) to an aprioric set of known spectra. [27]

The above model types require prior knowledge of the spectral sensitivities and the spectral power distribution (SPD) of the illumination. Measuring these spectral characteristics accurately is not a straightforward task, thus development of new estimation methods appeared. Such is the linear estimation model via least squares also known as the pseudo-inverse model, which is a modification of the Wiener estimation model that uses regression analysis between the known spectral reflectance's and the sensor responses. Imai-Berns model represents another model that doesn't assume prior knowledge of the spectral sensitivities and the SPD of the illumination. It also uses regression analysis between the output of the sensor and the weight column vectors for the ortho-normal basis vectors. [26]

Digital camera devices capture the spectrum by filtering the incoming color signal through a set of color filters [29]. Mathematically the interaction between the spectrum of the object, illumination and the digital camera can be modeled as follows:

$$P_i = \int_{\lambda} R(\lambda)\,\mathrm{E}(\lambda)S_i(\lambda)d\lambda + e_i \qquad (3.1)$$
$$i = 1,\ldots,m$$

, where $P_i(\mathrm{x},\mathrm{y})$ represents the response of the digital, $R(\mathrm{x},\mathrm{y};\lambda)$ is the spectral reflectance of an object, $E(\lambda)$ is the spectral power distribution of the illuminant, $\mathrm{S}_i(\lambda)$ represents the spectral camera sensitivity of the i^{th} camera channel , e_i is the camera system noise and λ is denoted as the wavelength variable. In practice, we have only three camera channels in a digital camera, namely the Red, Green and Blue channel, thus the m in equation 1 is equal to three.

3.1.1 Wiener estimation

Considering the case of the digital camera, the spectral reflectance of the image object is sampled uniformly at n intervals in the spectral range of 400 to 700 nm. Equation 1 can be more easily represented in a vector and matrix form as:

$$x = SEr + e \tag{3.2}$$

, where x is the camera response vector in a 3×1 column vector form, r is an $n\times1$ element column vector defined as $r = (\mathrm{R}(\lambda_1),...,\mathrm{R}(\lambda_n))^T$ and denotes the spectral reflectance of the objects, S is the spectral sensitivities matrix defined by a $3\times n$ matrix , E represents a $n\times n$ matrix corresponding to the illuminants SPD, and e is the 3×1 column vector denoting the noise. The noise is considered to be coming not only from the sensors but also the measurement errors of the spectral characteristics of the sensor, illumination and spectral reflectance. [26]

Reconstructing the r spectrum from the camera responses involves using aprioric information of the sensors, illumination and the reflectances of objects. This aprioric information is used so that the model learns from these in order to provide an estimation of the original r spectrum.

Let $M = SE$ be a simpler representation of the product of the spectral sensitivity of the camera and the SPD of the illumination.

The solution in reconstructing the reflectance spectrum is finding an estimation matrix W that minimizes the mean square error of the Euclid norm of $E\left\{\left\|r - Wx\right\|\right\}$, where $E\{.\}$ is defined as the expectation.

Matrix W is defined as:

$$W = R_{SS}M^T\left(MR_{SS}M^T + R_{EE}\right)^{-1} \tag{3.3}$$

, where

$$R_{SS} = E\left\{rr^T\right\}, \qquad R_{EE} = E\left\{ee^T\right\} \tag{3.4}$$

In equation3.3 and equation 3.4 T represents the transpose of a matrix, R_{SS} is the autocorrelation matrix of the spectral reflectance of the test or learning samples and R_{EE} represents the autocorrelation matrix of noise. If the autocorrelation matrices are equal to the actual autocorrelation matrices of noise and spectral reflectance, then the value of the MSE will be minimized [26]. Unfortunately this doesn't stand true because prior knowledge of noise is usually not available, and it is usually guessed.

The recovered spectrum has the form:

$$\hat{r} = Wx \tag{3.6}$$

The solution for Wiener estimation model involves the usage of aprioric knowledge which makes this method quite difficult. In a practical case, a more elegant solution is offered by the linear model via least squares fitting that recovers the spectral reflectance without the prior knowledge of the spectral sensitivities of the sensors and the SPD of the illumination [26].

3.1.2 Linear model via least squares fitting

The linear model via least squares represents a simple solution which is to build a mapping from camera responses to reflectance in order to minimize the least square error for a training set of known reflectance functions with known camera responses [41].

Thus we have a training set:

$$S = \left\{ \left(x_i, y_i \right), x_i \in \mathbb{R}^3, y_i \in \mathbb{R}^n, i = 1...m \right\} \tag{3.7}$$

This training set consists of the pairs of vectors corresponding to the camera responses x_i and the spectral reflectance y_i. The traditional setting method is characterized as estimating a set of three-dimensional scalar-valued functions as

$$\begin{aligned} y_i &= f_i\left(x\right), \\ i &= 1,...n \end{aligned} \tag{3.8}$$

, where y_i represents the reflectance at wavelength.

With every new set of camera responses x the reflectance is estimated by the associated functions $f_1\left(x\right), f_2\left(x\right), ... f_n\left(x\right)$. [27]

In the studied case there are only three channels corresponding to the camera responses, namely the red, green and blue channels. The input vector now becomes:

$$x = (R, G, B)^T \tag{3.9}$$

In practical cases x includes the constant variable 1, thus the input vector has the form:

$$x = (R, G, B, 1)^T \tag{3.10}$$

Given the input vector x we have the linear form:

$$f(x) = \langle w, x \rangle \tag{3.11}$$

The solution of w is searched so that the mean square error of the following is minimized:

$$L(f, S) = \|r - Xw\|^2 \tag{3.12}$$

, where X represents an $m \times 4$ matrix having each row as expressed in eq. and where r represents the reflectance vector, both X and r coming from the training set [27].

The solution for will have the form:

$$\hat{v} = (X^T X)^{-1} X^T r \tag{3.13}$$

, where $\hat{v}$ is the estimated spectral reflectance.

The estimates obtained in equation 3.13 and equation 3.6 are different because the estimates of the correlation and that of the noise are different [29].

3.1.3 Polynomial model via least squares fitting

The linear model can be extended to a nonlinear case by employing the polynomial spread of the camera responses. [27, 28]

The once linear function transforms to a nonlinear functions as:

$$f(x) = \langle w, \Psi^q(x) \rangle \tag{3.14}$$

, where the $\Psi^q(x)$ represents the input values now having the polynomial spread to the qth degree of the polynomial terms.

The solution in this case will have the form:

$$\hat{v} = \left(P^T P\right)^{-1} P^T r \tag{3.15}$$

, where $\hat{v}$ is the estimated spectral reflectance and P is a matrix having each row an input vector of $\Psi^q(x_i)$

3.1.4 Special considerations

Because of the large amount of information present in the data-cube, the storage size of a spectral image is quite high amounting to hundreds of megabytes or even gigabytes. This can pose a problem when considering creating an application for a smartphone that retrieves and stores the spectral data. Therefore special consideration needs to be given for this. Usually, the spectral image data-cube is saved to user specific binary formats, or different compression methods are used like PCA in order to reduce dimensionality [54-56].

Another fact to consider is also memory allocation, as estimation methods work using large matrixes in order to construct the data cube. There has to be a good balance between correct allocation of memory resources and time spent in obtaining the spectral image. So considering the case of a 20 megabit sensor we will have a 4000x5000x3 RGB image. When transforming it to a spectral image considering the visible range of 400-700nm with 5 nm sampling we will get 4000x5000x61 data cube. This occupies roughly more than 1Gb of memory space. Reducing dimensions of the spectral image data cube can be done by choosing an optimal sampling. This is of course illuminant [79] and application dependent. Also as previously mentioned reducing the spectral data can be done by different compression methods like PCA.

3.2 Spectral metrics

In order to measure the distance between the original spectral reflectance and the estimated spectral reflectance two different spectral metrics were used: goodness of fit coefficient (GFC) and root mean square error (RMSE). These metrics are good for distinguishing between metamers. However they do not consider human vision [40]

3.2.1 Goodness of fit coefficient (GFC)

In order to evaluate the goodness of the mathematical reconstruction, the GFC is used which is based on Schwartz inequality:

$$GFC = \frac{\left|\sum_i R_m(\lambda_i)\,\mathrm{R}_e(\lambda_i)\right|}{\sqrt{\left|\sum_i \left[R_m(\lambda_i)\right]^2\right|}\sqrt{\left|\sum_i \left[R_e(\lambda_i)\right]^2\right|}} \tag{3.16}$$

, where, $R_m(\lambda_i)$ represents the original measured spectral reflectance at wavelength (λ_i) and $R_e(\lambda_i)$ represents the estimated spectral reflectance at wavelength (λ_i).

The GFC coefficient takes values ranging from 0 to 1, with the value 1 having the meaning that the estimate represents the exact spectra of the original. For colorimetric accuracy $R_e(\lambda_i)$ needs the GFC to be higher than 0.995. For good spectral fit the GFC needs to be $GFC \geq 0.999$ and $GFC \geq 0.9999$ is considered as almost perfect fit. [35-39]

3.2.2 Root Mean Square Error (RMSE)

RMSE represents another way of computing the differences between the original spectra and the estimated spectra. As the name implies it gives the squared error loss by calculating the square root of mean square error [35-39].

$$RMSE = \sqrt{\frac{1}{N}\sum_{i=1}^{N}\left\|R_m(\lambda) - R_e(\lambda)\right\|^2} \tag{3.17}$$

Where $R_m(\lambda)$ represents the original spectra and $R_e(\lambda)$ represents the estimated spectra and N is the number of elements in the spectra.

3.2.3 CIELAB Color Difference

Psychophysical experiments have shown that the human eye's sensitivity to light is not linear [50]. The RGB and also the XYZ color spaces defined by the CIE (International Commission on Illumination) are linearly related to the spectral power distribution of the colored light. When changing the tristimulus values XYZ (or RGB) of a color stimulus, the observer will perceive a difference in color only after a certain amount, equal to the Just Noticeable Difference (JND). [50] In both RGB and XYZ spaces the JND depends on the location in the color spaces. In order to address this CIELAB space was proposed in 1976 by CIE, having the quantities: [51]

$$\begin{aligned} L^* &= 116 f\left(\frac{Y}{Y_n}\right) - 16 \\ a^* &= 500\left[f\left(\frac{X}{X_n}\right) - f\left(\frac{Y}{Y_n}\right)\right] \\ b^* &= 500\left[f\left(\frac{Y}{Y_n}\right) - f\left(\frac{Z}{Z_n}\right)\right] \end{aligned} \tag{3.18}$$

$$\begin{aligned} f\left(\frac{K}{K_n}\right) &= \left(\frac{K}{K_n}\right)^{\frac{1}{3}} \; if \; \frac{K}{K_n} > \left(\frac{24}{116}\right)^3 \\ f\left(\frac{K}{K_n}\right) &= \left(\frac{841}{108}\right)\left(\frac{K}{K_n}\right) + \frac{16}{116} \; if \; \frac{K}{K_n} \leq \left(\frac{24}{116}\right)^3 \end{aligned} \tag{3.19}$$

, where K can be each of the three tristimulus values X, Y, Z and X_n, Y_n, Z_n represent the tristimulus values of a perfect reflecting diffuser under the same illuminant. The values are normalized so that $Y_n = 100$.

L^* represents the lightness of a color going from a scale of 0 (black) to 100 (white). Chromaticity can be represented on a 2D diagram where a^* is the degree of red versus green and b^* is degree of yellow versus blue.

CIELAB color difference is defined in the CIELAB color space system as the Euclidean distance between two color stimulus with the following equation [46, 47, 51]:

$$\Delta E^* = \sqrt{(\Delta L^*)^2 + (\Delta a^*)^2 + (\Delta b^*)^2} \tag{3.20}$$

$$\begin{aligned} \Delta L^* &= L^*_1 - L^*_2 \\ \Delta a^* &= \tilde{a}_1 - \tilde{a}_2 \\ \Delta b^* &= b^*_1 - b^*_2 \end{aligned} \tag{3.21}$$

Practical interpretations of ΔE^* can be found in tables in the works of Hardeberg et al [49] and Abrado et al [48], and can be seen in tables below:

Table 1 Interpretation of CIELAB color difference by Abrado et al [48]

$\Delta\tilde{E}$	Effect
0-1	Limit of perception
1-3	Very good quality
3-6	Good quality
6-10	Sufficient
>10	Insufficient

Table 2 Interpretation of CIELAB color difference by Hardeberg et al [49]

$\Delta\tilde{E}$	Effect
<3	Hardly perceptible

3-6	Perceptible, but acceptable
>6	Not acceptable

3.2.4 CIEDE2000 Color difference

CIEDE2000 is a CIE recommended color difference formula, which includes new terms to improve the predicted color difference in the blue region and for neutral colors, for pairs of samples with small to moderate color differences [52]. CIEDE2000 is based on the CIELAB color space. Given a pair of color values in CIELAB space $\{L_i^*, a_i^*, b_i^*\}_{i=1}^2$, the CIEDE2000 color difference between them is calculated using the equation:

$$CIEDE2000 = \sqrt{\left(\frac{\Delta\tilde{L}}{k_L S_L}\right)^2 + \left(\frac{\Delta\tilde{C}}{k_C S_C}\right)^2 + \left(\frac{\Delta\tilde{H}}{k_H S_H}\right)^2 + R_T\left(\frac{\Delta\tilde{C}}{k_C S_C}\right)\left(\frac{\Delta\tilde{H}}{k_H S_H}\right)} \quad (3.22)$$

3.3 JPEG compression

As previously mentioned the output of the majority of commercial digital cameras is presented in different formats rather than the direct sensor output. Usual formats that can be found imply some form of compression such as JPEG data type, PNG data type or TIFF data type.

Smartphone cameras also include as the main form of output JPEG type images. Newer generation of camera sensors are being developed such to allow access to the RAW information. Currently only the Nokia PureView technology allows the direct sensor output [75]. However still the main form as output remains the JPEG image as it represents a storage cost effective compression method that discards information that the human eye cannot easily see.

JPEG is the international standard for the effective compression of the still digital images. It includes specifications for both- lossless and lossy compression algorithm. JPEG lossy standard was designed with the consideration to diminish the high frequency component of the image frame that human eye cannot detect easily. This was done due to the fact that human vision detects better changes in the light intensity rather than changes in color space. JPEG standard tends to be more aggressive towards the compression of the color-part (chrominance) of the image instead of the gray-scale part of the image. Compression in JPEG is realized mainly due to the quantization effect, which when implemented results in the loss of part of the image information and hence degradation of image quality occurs [74].

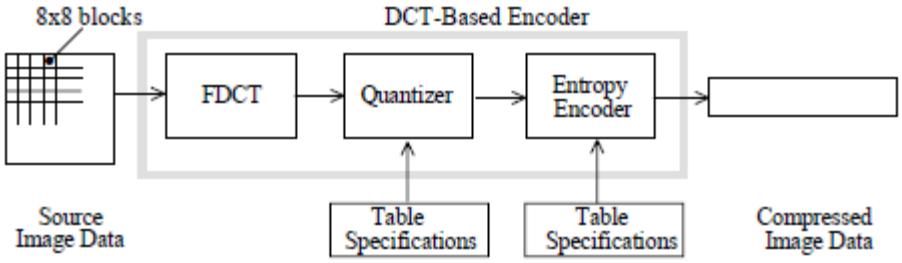

Figure 11 Steps in implementing the JPEG encoder [77]

Figure 10 presents the steps involved in implementing the JPEG encoder. The first step involves transforming the image to an appropriate luminance/chrominance color space such as YCbCr space. The grayscale, low frequency component Y contains the luminance information of the image to which human eyes are sensitive. The other channels Cb and Cr are chrominance channels that contain the high frequency color information to which human eyes are not sensitive in the blue and red region. As the chrominance channels contain less relevant information they are usually subsampled. Typical patterns (as seen in Figure 11) include subsampling the chrominance channel in vertical direction (4:2:2), or horizontal direction (4:4:0) or both (4:2:0) [76]. All processing after this is done on each channel individually.

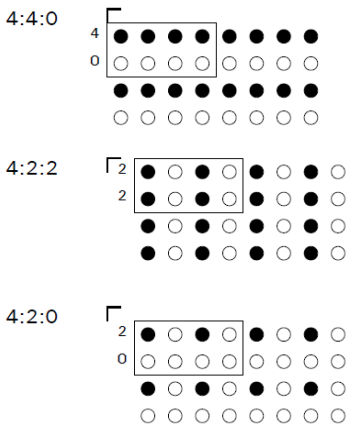

Figure 12 Type of chroma channel subsampling (4:4:0), (4:2:2) and (4:2:0) [76]

The next step involves splitting the channel image in 8x8 blocks as all the subsequent steps of JPEG algorithm are performed on them.

Next, the Discrete Cosine Transform(DCT) is applied (having the mathematical form expressed in Equation 3.23), where the spatial form of the image is now converted to a frequency domain representation so that it is a more convenient to discard the high frequency components that. In the resulting 8x8 matrix after the DCT, the coefficient with zero frequency is called the DC coefficient, while the rest 63 are called AC coefficients [78].

$$F(u,v) = \frac{1}{4} C(u) C(v) \left[\sum_{x=0}^{7} \sum_{y=0}^{7} f(x,y) * \cos \frac{(2x+1)u\pi}{16} \cos \frac{(2y+1)v\pi}{16} \right] \quad (3.23)$$

, where

$$f(x,y) = \frac{1}{4} \left[\sum_{u=0}^{7} \sum_{v=0}^{7} C(u) C(v) F(u,v) * \cos \frac{(2x+1)u\pi}{16} \cos \frac{(2y+1)v\pi}{16} \right]$$

, and

$$C(u), C(v) = \frac{1}{\sqrt{2}} \quad for\, u, v = 0$$
$$C(u), C(v) = 1 \quad otherwise$$

After this follows the most important step in the JPEG compression, namely the quantization, as it is the principal source of lossiness. This is done by dividing each of the DCT coefficients by a quantization table and then rounding the result. Thus the high frequency DCT coefficients are quantized more heavily, in comparison with the low frequency coefficients, as the play a smaller role in the image representation and cannot be easily perceived by human eyes. Quantization tables are defined as user specific. [78]

After quantization, the DC coefficient is treated separately from the 63 AC coefficients. The DC coefficient is a measure of the average value of the 64 image samples. The DC coefficient is encoded as the difference from the DC term of the previous block in the encoding order. After all of the quantized coefficients are ordered into the "zig-zag" sequence. This ordering helps to facilitate entropy coding by placing low-frequency before high-frequency coefficients [77].

The final processing step is entropy coding. This step achieves additional compression losslessly by encoding the quantized DCT coefficients more compactly based on their statistical characteristics. The JPEG proposal specifies two entropy coding methods - arithmetic coding and Huffman coding, where the latter is used in baseline sequential JPEG encoding [77].

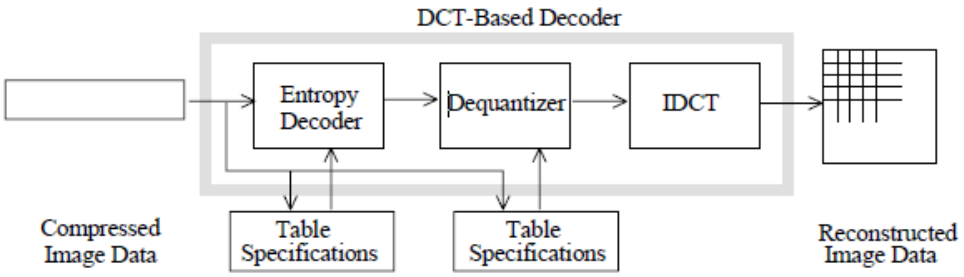

Figure 13 Steps in implementing the JPEG decoder[77]

In order to decode the JPEG compressed data, the JPEG decoder is needed. This basically reiterates all the mentioned processing steps in a reverse order (as seen in Figure 12). Thus we will have an entropy decoder, a dequantizer, and an Inverse Discrete Cosine Transform (IDCT) that will reconstruct the image data

4 Measurements

4.1 Data acquisition

4.1.1 Specim ImSpector (V10E)

In order to capture the true reflectance of the mentioned samples the Specim ImSpector (V10E) spectrograph was used.

The Specim ImSpector V8E [43] (Figure14) is designed for the VIS wavelength range. This spectrograph provides a straightforward, high performance and cost-effective method of integration in machine vision systems. When combined with scientific grayscale CCD or CMOS cameras, the combination provides a line-scan Spectral Imaging device. In this study the latter case was considered. An imaging spectrometer instrument (or spectral imaging instrument), based on an imaging spectrograph such as this one can be defined as an instrument capable of simultaneously measuring the optical spectrum components and the spatial location of an object surface.

As key features of the device, we can list the following:

- Spectral range: 400-1000nm
- Spectral resolution of 2.8 nm (with 30 μm slit).
- Image size: 6.15 (spectral) * 14.2 (spatial) mm.
- Spatial resolution: rms spot radius <9 μm.
- No astigmatism.
- Numerical aperture F/2.4.
- Optical input: Telecentric
- Efficiency over 50% (independent of polarization).

Figure 14 Specim ImSpector (V10E) spectrograph [44]

The combination of the spectrograph and CCD sensor as line scanning camera provides as output, a 2D spectral image data-cube, which is obtained after the target is scanned line by line in one spatial direction.

Measurement setup

The geometry used was a variation of the standard 45/0 geometry. In this case, the setup is composed by two incandescent lamps placed equidistantly from the sample, at 45 degrees angle from the sample's normal in the vertical direction (as seen in Figure 15). Then, the spectral signal coming from the sample's surface enters through an optical system which then splits it: one ray entering ImSpector V10E and the other one entering another spectral line camera. This second device is not considered in this study.

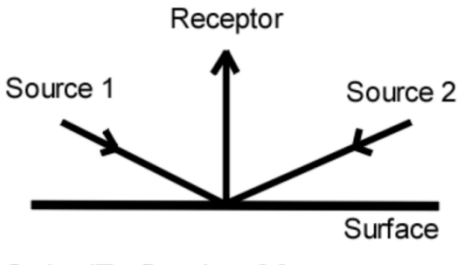

Figure 15 Measurement setup for ImSpect V10E

Device calibration

Prior to taking the measurements device calibration was done.

First a saturation check of the sensor was performed, which translates into setting specific exposure time. As such a white diffuse reference sample was introduced and the appropriate exposure time was selected. The exposure time considered for the ImSpector V10E was 58 ms.

Also the raw images acquired by the camera had to be pre-processed to correct for the measurement deficiencies inherent to the acquisition system. The corrections needed are:

- A dark current correction (a dark current image is taken $Dark_{im}$)
- A detector calibration, performed by measuring the mentioned white diffuse reference sample White_{im} .

The final image is calculated from the captured image $\mathrm{Im}_{captured}$ and the two compensation images according to the following equation [45]:

$$\mathrm{Im}_{final} = \frac{\mathrm{Im}_{captured} - Dark_{im}}{White_{im} - Dark_{im}} \tag{4.1}$$

After the image data cube was created, spectral patch corresponding to each individual sample was selected. From each patch the spectral reflectance of the sample was obtained by averaging all the spectral reflectances corresponding to each pixel in the patch. Also the spectral range of the measurement was shortened from a range of 400-1000nm to the visible range of 400-700nm with a sampling rate of 10nm.

4.1.2 RGB cameras

Capturing the RGB data which will be further used in the estimation methods was done using seven digital cameras. These comprised four smartphone cameras, two DSLR cameras and one simple commercial digital camera.

Table 3 shows some key figures of the cameras. It is important to notice that all the smartphone cameras and the commercial digital camera considered have a back-illuminated CMOS sensor, while the DSLR come with simple CCD and CMOS sensors. The BSI CMOS type sensors were considered in the smartphone cameras by manufactures in order to improve to light sensitivity incident to the small sensors. Other features presented in the table include camera resolution, focal length, aperture and camera image formats. All the cameras considered have the ability to capture JPEG type of image formats, while obtaining the RAW type data is possible just for the DSLR and one mobile camera, namely the one belonging to the Nokia 1520.

Table 3 RGB digital camera devices used

Camera	Sensor type	Sensor size (inch)	Sensor pixel size (µm)	Camera full resolution (megapixels)	Focal length of system (mm)	Optical F/# Aperture	Camera image formats
Iphone 5S	CMOS BSI	1/3	1.5x1.5	8	-	f/2.2	JPEG
HTC One	CMOS BSI	1/3	2x2	4	3.82	f/2.0	JPEG
Samsung Galaxy S2+	CMOS BSI	-	-	8	-	f/2.6	JPEG
Olympus TG1	CMOS BSI	½.3	-	12	-	f/2.0-f/4.9	JPEG

Nokia 1520	CMOS BSI	½.5	1.12x1.12	20	26	f/2.4	JPEG, 10 bit RAW
Nikon D80	CCD	23.6x15.8 milimeter	-	10	-	f/3/5-f/5.6	JPEG, TIFF, 12 bit RAW
Nikon D800	CMOS	35.9x24 milimeter	0	36	-	f/3/5-f/5.6	JPEG, TIFF, 14 bit RAW

Measurement setup

The RGB images were capture in the light booth using a D65 illumination, and the surround was kept dark. The geometry considered was 45/0, where the samples were illuminated at a 45 degree angle, while the measurements of the samples were captured at a 0 degree angle (as seen in Figure 16). The geometry was chosen so that the specular components of the samples did not appear in the images.

When capturing the images some parameters were fixed such as the ISO set to 100 (in the HTC One case this was not possible even though the setting allowed so), distance from target to 40cm and auto white balancing. Other parameters were considered inherent as it was not possible to change them such as the resolution, exposure time, and aperture. Only the DSLR cameras allowed changing aperture and exposure time, thus the values selected were so that the ratio between the exposure time and aperture was similar to the ones obtained in the mobile cameras. All numerical values can be seen in Table 4.

The images considered in tests were both JPEG and RAW in the cases where the camera allowed so.

All the parameters considered were established so that it was possible to provide similar results in the image capturing process, which will allow further on a comparison between the different devices.

Figure 16 Measurement setup for RGB cameras

Table 4 Camera parameters considered when RGB data was measured

Camera Setup	ISO	Distance from target	Camera full resolution (megapixels)	Exposure time (in sec)	Optical F/# Aperture	Camera image formats
Iphone 5S	100	40cm	8	Auto-1/100	f/2.2	JPEG
HTC One	100-160	40cm	4	Auto – 1/107	f/2.0	JPEG
Samsung Galaxy S2+	100	40cm	8	Auto – 1/27	f/2.6	JPEG
Olympus TG1	100	40cm	12	Auto – 1/60	f/2.0	JPEG
Nokia 1520	100	40cm	20	1/40	f/2.4	JPEG, 10 bit RAW
Nikon D80	100	40cm	10	1/20	f/5	JPEG, TIFF, 12 bit RAW
Nikon D800	100	40cm	36	1/20	f/5	JPEG, TIFF, 14 bit RAW

Data normalization

Before using the captured RAW images for further study, they suffered some post processing steps which include:

- Correction of noise by averaging multiple shots of object image. More specifically five images were taken of the data charts and were averaged.

- Correction of the non-uniformity of the illumination in the sensitivities of each pixel. In this process we acquired the normal image, an image of a white diffused reference sample and a dark image (by taking the image with the lens cap on). The correction is done using the formula [45]:

$$\hat{I}_{i,j,k} = \frac{I_{i,j,k} - D_{i,j,k}}{W_{i,j,k} - D_{i,j,k}} \tag{4.2}$$

,where $I_{i,j,k}$, $W_{i,j,k}$, $D_{i,j,k}$, $\hat{I}_{i,j,k}$ represent respectively the sensor response to an imaged data samples, a sensor response to the white diffused reference, the sensor response of a dark signal and a corrected sensor response of the imaged data samples for the k^{th} channel and at the spatial position (i, j).

Device characterization

In order to completely characterize the sensors of the devices used, the camera sensitivities were measured following a classical setup as seen in Figure 17.

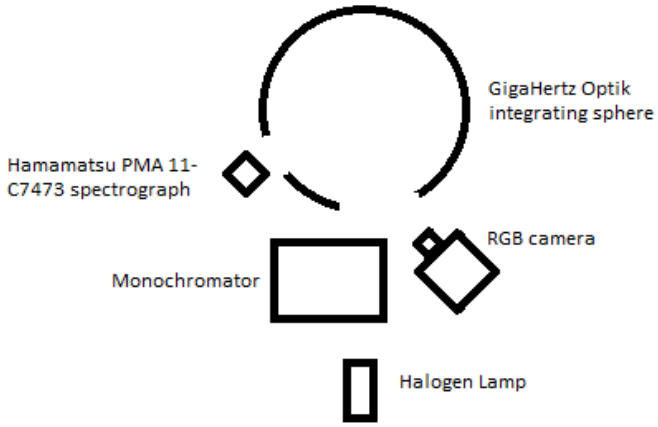

Figure 17 Cameras sensitivity measurement setup

The setup used for the camera sensitivity measurements consists of a GigaHertz Optik Integrating Sphere of a diameter of 500mm, a monochromator with a halogen light source, a Hamamatsu PMA11-C7473 optical fiber spectrometer and the camera imaging system. The RGB camera was placed in front of the integrating sphere at a 45 degree angle and focused inside the sphere. The sphere was illuminated with light coming from the halogen lamp impinging through the monochromator placed at a 0 degree angle. The monochromator was set to the spectral range of 380 to 700nm with a 10nm wavelength step, giving in total 33 wavelengths.

For each wavelength the radiant flux was measured with the spectrometer and a RGB image was acquired from the camera. All 33 wavelengths were measured and imaged one by one. The sensitivities were obtained by dividing the sensor response of each of the three channels with the measured radiant flux of the light. Afterwards the values were scaled by dividing to the maximum found value.

Normally the sensitivity of a camera is calculated using the RAW type file data. This is of course an important step in characterizing the cameras sensor and also represents essential information as it is needed in different estimation models, as seen in Chapter 3.

JPEG type data is not used in sensitivity measurements as it is quite different from the raw data, because it suffers from many post-processing steps such as: white balance, color interpolation, color correction, gamma correction, color space conversion, saturation enhancement, etc. Unfortunately smartphone camera manufacturers regard sensitivity characterization of a sensor as a close guarded secret therefore making it unavailable. The ability to capture raw unaltered sensor data is still not yet widely available for smarphone cameras, currently only some Nokia devices having this ability.

Therefore measuring the sensitivity from JPEG images has been performed, starting from the idea that different smart-phone camera manufacturers use different post-processing methods, this in turn allowing to obtain some usable data in terms of sensitivity measurements. This was done also in order not to limit the estimation methods that can be employed.

Results are shown in Figures 18 and 19.

Figure 18 presents camera sensitivities measured from RAW and JPEG type image from Nokia 1520, Nikon D80, and Nikon D800. As expected the results show clearly that there is a big difference from the sensitivities obtained from the RAW data and the ones obtained from the JPEG data. In case of the Nikon cameras we see that in the green region the sensitivities are lower, when obtained from the JPEG images. We also see that the blue and red regions show enhanced sensitivity when obtained from the JPEG images. This fact is also seen in the case of Nokia 1520 camera. This is of course due to post-processing block, which has the task to modify the images in order to provide the user a visual pleasant image.

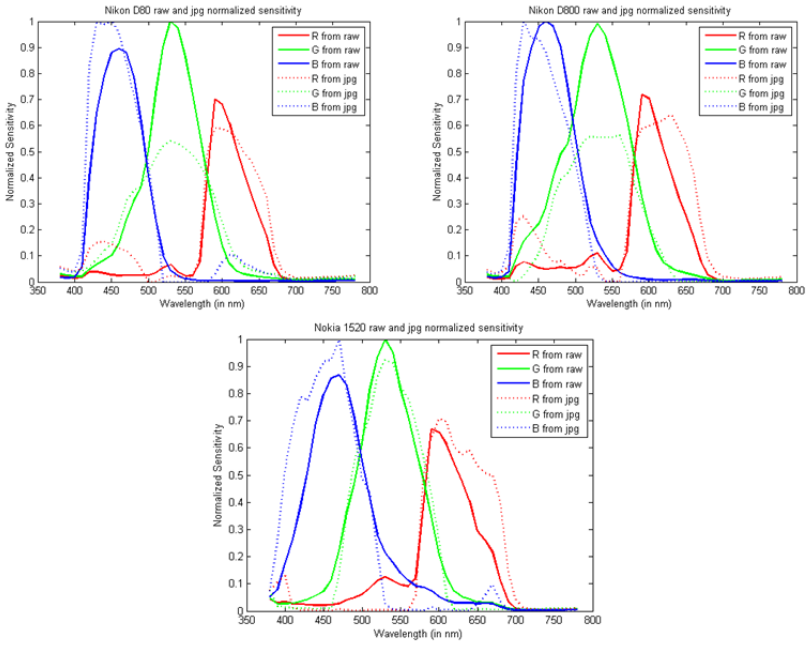

Figure 18 Sensitivities obtained from RAW and JPEG type images Nikon D80, Nikon D800 and Nokia 1520

Figure 19 shows the camera sensitivities for the devices where the JPEG output was available. In this case the sensitivities have very rough shapes and fluctuating values. This can be especially seen in the HTC One case.

Results seen show, as expected, that evaluating the sensitivities from the JPEG type output of the smartphone cameras, and also DSLR cameras do not provide accurate results. This in turn means that there will a limitation in the estimation methods used for reflectance estimation. Because of this further evaluations of the smartphone devices in obtaining the spectral data will be done using just the liniar fitting via least squares method and the polynomial fitting via least squares method described in Chapter 3.

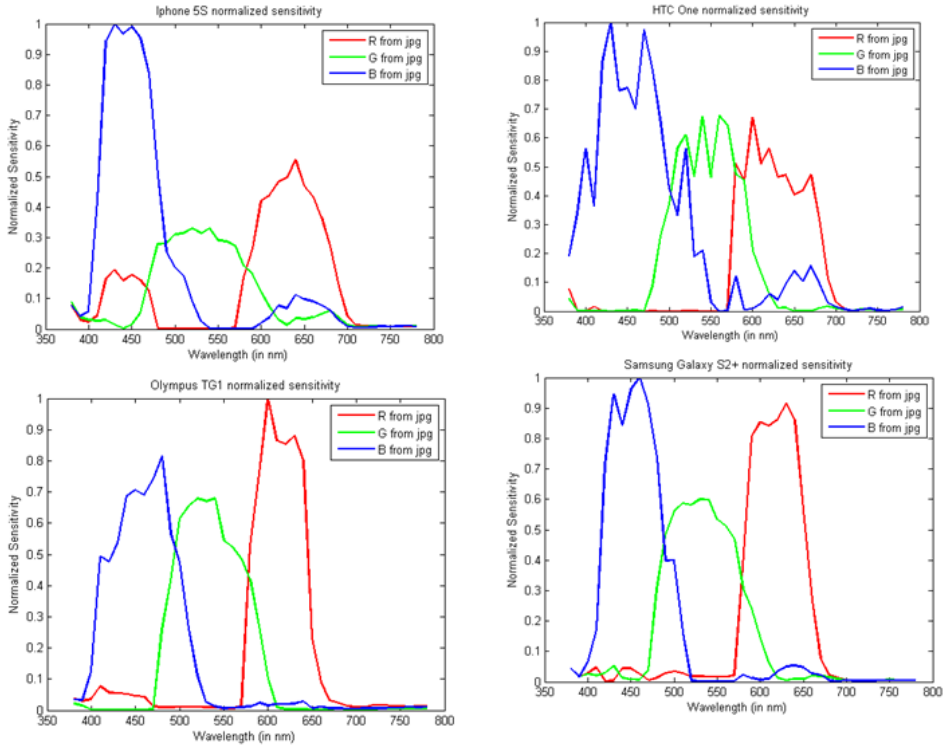

Figure 19 Sensitivities obtained from JPEG type images for IPhone 5S, HTC One, Olympus TG1, and Samsung Galaxy S2+

4.2 Samples

To evaluate the reflectance reconstruction on the camera devices in detail, the experiments were conducted on two charts: a classical Xrite Color Checker Digital SG and natural materials chart. The Xrite Color Checker Digital SG was used to study the influences of JPEG type compression and image processing block upon reconstructing the spectra on said devices. The natural material chart was used to study how the smarphones cameras perform in terms of reflectance estimation and also to provide a comparative study of their performance against the DSLR cameras.

4.2.1 Xrite ColorChecker Digital SG chart

The ColorChecker Digital SG chart (Figure 20) includes the colors from the standard ColorChecker target, many of which represent natural objects, such as human skin tone, foliage and blue sky. Also it includes additional skin-tone reference colors for a wide variety of skin tones [41]. Out of the 140 patches of the Digital SG color checker only 96 of them were selected in the tests.

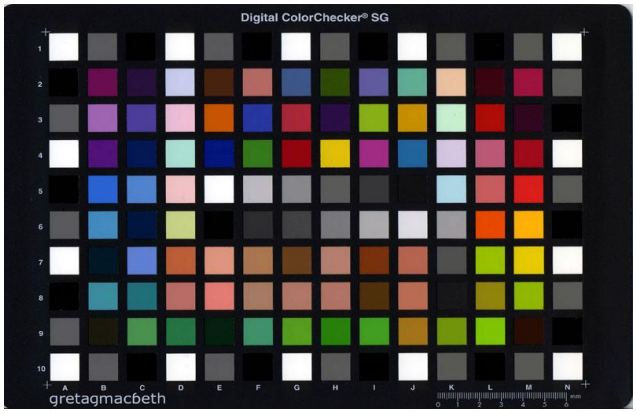

Figure 20 XriteColor Checker Digital SG

4.2.2 Natural material chart

The second sample set used for estimation of reflectances is a material chart. This was first developed as part of the Industrial Project course which had the task of waste sorting through different machine vision techniques.

The material chart is composed of 100 samples collected in Joensuu (Finland). It includes different types of newspapers, magazines, food packaging, cans, plastic bottles, caps, yoghurt cups, stones, wood, construction debris, etc. The plastic samples include several types of polymers (e.g. PP, PS, PET. . .), and not all of them are marked with the Plastic Identification Code (PIC).

The samples have been cut to a size of about 1 x 1 cm and have been glued on a board in a matrix fashion, having 10 rows and 10 columns. The samples were selected so as to be classified into five main classes: paper, plastic, metal, wood and stone. Each of the five main classes contain elements on two rows, therefore the first two rows correspond to the paper category, the next two rows correspond to the plastics category, etc. (as seen in Figure 21.) Also the samples were selected so as to have a flat surface in order to be more appropriate for some measurement devices.

Figure 21 Natural material chart

In the experiments done samples from both charts were used as testing sets for estimation, while as training samples for estimation only the XriteColor Checker Digital SG was used.

5 Experiments and Results

5.1 Testing how JPEG compression rate affects estimation in smartphones

An important part in examining the usability of the smartphone as a pocket spectral imaging device was to study how the JPEG files that come as output for today mobile sensors affect the recovery of the spectral data. There are already evaluations that prove that RAW files provide clearly better results than JPEG files in terms of reflectance estimation [XXX]. However the study in this case was made in order to provide a better understanding on the type of situations and challenges that will allow a smartphone camera to become a pocket spectral imaging device.

In order to address this first problem an experiment was done. For this, the three cameras that allowed capturing the RAW images were used: Nikon D80, Nikon D800 and the smartphone camera Nokia 1520. The raw images were that of the Xrite Color Checker Digital SG.

From these RAW images using the JPEG algorithm presented in chapter 3.3, three JPEG files were created for each RAW image using different compression ratios based on a quality type compression: 100% quality, 75% quality and 50% quality. So in total there were 3 raw images and 9 newly created JPEG images.

When creating the JPEG quality type compressed images the main elements that lead to the compression was the (4:2:0) chroma subsampling the quantization of the DCT coefficients. In order to create the three types of quality ratios the standard quantization tables for luminance and chrominance were modified using the algorithm:

```
qf = 100 ;              % 75, 50 quality
if qf < 50
   q s c a l e = f l o o r (5000 / qf) ;
else
    q s c a l e = 200 - 2 * qf ;
end
q y = round (q y  *q s c a l e / 1 0 0)
q c = round (q c * q s c a l e / 1 0 0)
```

Figure 22 shows the new quality based quantization tables that were used in creating the new images.

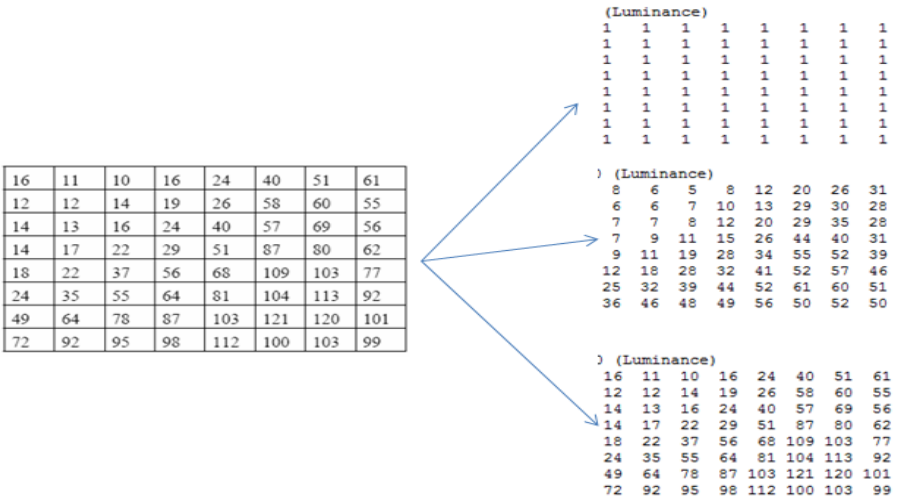

Figure 22 Conversion of Luminance quantization table into new quality based quantization tables (Upper table represents 100% quality, middle 75% quality and last table represents 50%)

Once obtained the JPEG type images reflectance estimation was performed. The estimation methods employed are the ones presented in chapter 3 liniar fitting via least squares and polynomial fitting via least squares. The samples used in estimating the spectral reflectance were the 96 samples of the Xrite Color Checker Digital SG. For this Leave One Out (LOO) evaluation was performed where 95 samples were used as training samples and 1 sample as test. This was done for all color chart samples.

As results are similar for all the considered devices (Nikon D800, Nikon D80 and Nokia 1520), shown next are just the results for Nokia 1520 smartphone camera, while the rest are included in Annex.

5.1.1 Results for spatial homogenous case

Figure 23 show the RMSE wavelength-wise errors for liniar fitting between the RAW and JPEG quality type images for the Nikon D80, Nikon D800 and Nokia 1520. At first glance we notice that independent of the device the RMSE wavelength-wise error maintains the same shape for both the RAW and the JPEG images. The shape of the RMSE wavelength-wise error can be easily explained by considering the sensitivity curves of the sensor used. Thus looking again at Figure 23 we see that highest error peaks correspond to the places where the sensor does not have sensitivity, such as the ends of the spectrum (beginning of the 400nm region and region from 640nm onwards) , and the regions where the sensitivity of the sensor intersects (at 500nm and 570nm).

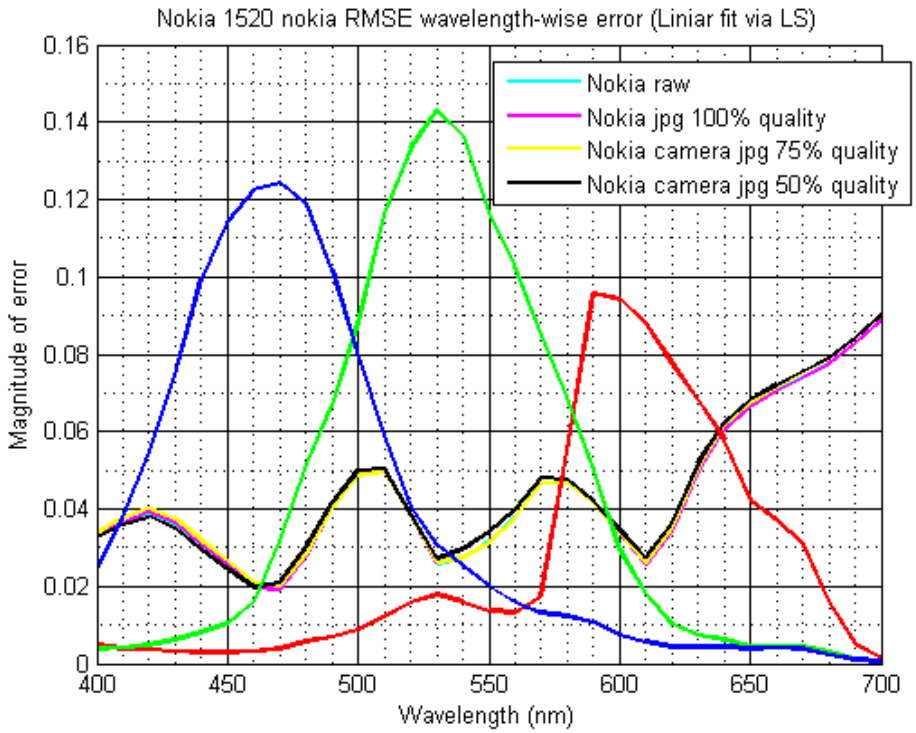

Figure 23 RMSE wavelength-wise error (Liniar fit via LS) for Nokia 1520 in testing the influence of JPEG compression in reflectance estimation (spatial homogenous case)

Table 6 showing the RMSE and GFC error measures confirms the initial result that the spectral reconstruction obtained from the RAW image is very similar to the one obtained from JPEG quality scale images.

Table 5 however paints another picture. We see that from a colorimetric point of view the reflectance estimation in the case where RAW image was used provided better color difference results. While the mean color differences when using the 100% quality JPEG is very close the one obtained from the raw, we see that the maximum is quite different. The 50% and 75% quality JPEG images show a steady increase in color difference error.

Table 5 CIELAB and CIEDE2000 results for liniar fitting in testing the influence of JPEG compression in reflectance estimation (spatial homogenous case)

	CIELAB				CIEDE2000			
	Min	Mean	Max	Standard deviation	Min	Mean	Max	Standard deviation
Nokia raw	0.5	4.1	11.6	2.5	0.3	2.6	11.6	1.9
Nokia JPEG	0.5	4.3	14.3	2.8	0.2	2.7	13.1	2.1

100%								
Nokia JPEG 75%	0.5	5.0	17.6	3.4	0.3	3.1	13.5	2.5
Nokia JPEG 50%	0.4	5.5	23.7	4.4	0.3	3.3	18.1	3.0

Table 6 RMSE and GFC for liniar fitting in testing the influence of JPEG compression in reflectance estimation (spatial homogenous case)

	RMSE				GFC			
	Min	Mean	Max	Standard deviation	Min	Mean	Max	Standard deviation
Nokia raw	0.008	0.042	0.149	0.022	0.718	0.976	0.999	0.041
Nokia JPEG 100%	0.008	0.042	0.149	0.022	0.721	0.976	0.999	0.041
Nokia JPEG 75%	0.008	0.042	0.153	0.022	0.721	0.975	0.999	0.043
Nokia JPEG 50%	0.009	0.043	0.146	0.021	0.696	0.974	0.999	0.045

When considering the case of spectral estimation via polynomial fitting the results stay the same, in the sense that there is very little difference spectrally between the estimation done with the RAW images and the one done JPEG quality based images (see Figure 24 and Table 8). The color differences also show the same information as previously, that there is a difference between results obtained with the RAW and those obtained with JPEG images.

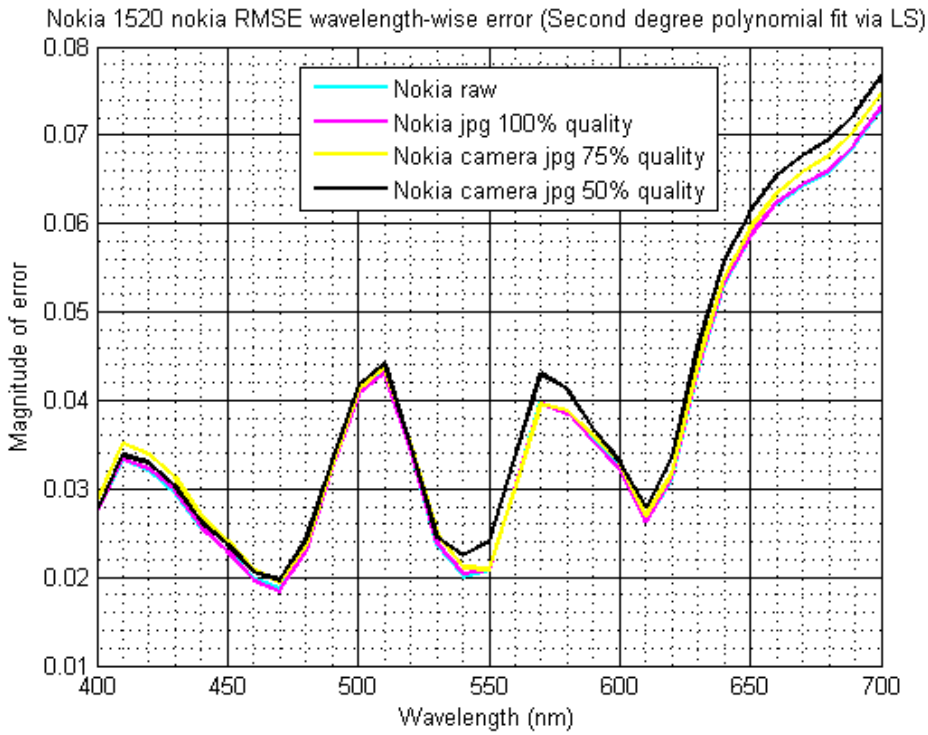

Figure 24 RMSE wavelength-wise error (Second degree polynomial fit via LS) for Nokia 1520 in testing the influence of JPEG compression in reflectance estimation (spatial homogenous case)

Table 7 CIELAB and CIEDE2000 for second degree polynomial fitting in testing the influence of JPEG compression in reflectance estimation (spatial homogenous case)

	CIELAB				CIEDE2000			
	Min	Mean	Max	Standard deviation	Min	Mean	Max	Standard deviation
Nokia raw	0.5	3.7	10.7	2.3	0.3	2.1	6.5	1.1
Nokia JPEG 100%	0.3	3.8	12.3	2.7	0.2	2.2	9.2	1.3
Nokia JPEG 75%	0.9	4.5	15.4	3.0	0.7	2.6	9.9	1.5
Nokia JPEG 50%	0.6	5.0	17.9	3.7	0.4	3.0	14.5	2.2

Table 8 RMSE and GFC for second degree polynomial fitting in testing the influence of JPEG compression in reflectance estimation (spatial homogenous case)

	RMSE				GFC			
	Min	Mean	Max	Standard deviation	Min	Mean	Max	Standard deviation
Nokia raw	0.007	0.036	0.119	0.018	0.771	0.98	0.999	0.029
Nokia JPEG 100%	0.007	0.036	0.118	0.018	0.774	0.984	0.999	0.030
Nokia JPEG 75%	0.008	0.037	0.123	0.019	0.793	0.983	0.999	0.030
Nokia JPEG 50%	0.009	0.037	0.112	0.020	0.733	0.982	0.999	0.035

The results obtained showing that RAW images and JPEG images provide similar spectral estimations should be considered with certain reservations. This is because we were considering the ideal homogenous case where the samples were simple color patches and not samples with great level of detail and color variations. As already mentioned we know that JPEG compression affects the image data mostly on the high level frequencies which corresponds to level the details in the image. Reducing the quality of the JPEG image means discarding more high level frequencies and implicitly the details of the image.

Also another important cause for this result is that the spectral reflectance of the samples was obtained through a great deal of averaging. After the spectral estimated image data cube was obtained, a 30X30 patch of each sample was extracted and averaged in order to obtain the spectral reflectance of the sample.

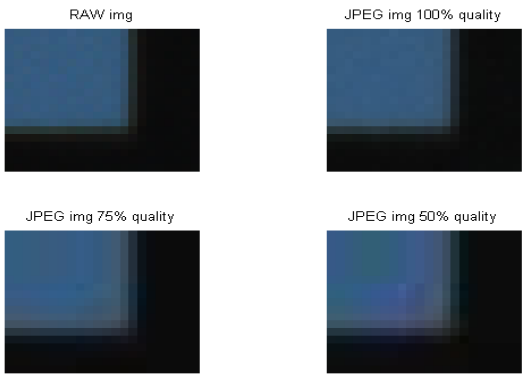

Figure 25 Image showing variations in the level of detail between RAW and JPEG images with different compression ratios

5.1.2 Results for spatial non-homogenous case

Thus in order to consider a real case scenario where we don't have the ideal homogenous case, the reflectance spectra was recovered this time by considering the RGB data from the corners of the samples where now we see variations in the level of detail and color (Figure 25). Also less averaging was done, now using just a 3x3 patch to obtain the estimated spectra of the samples.

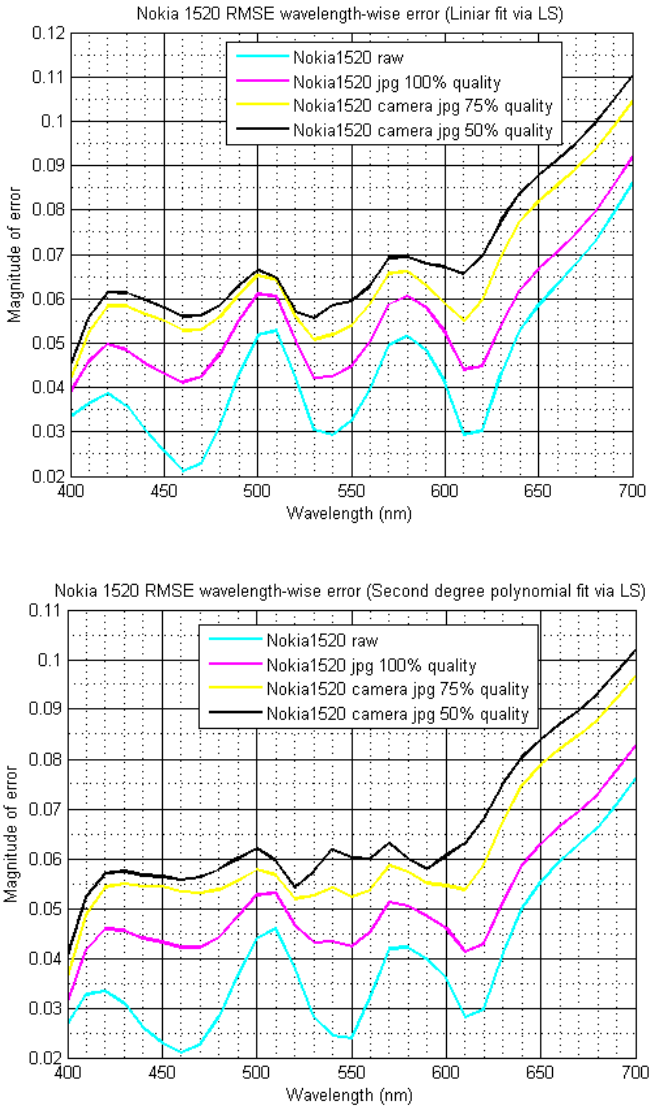

Figure 26 RMSE wavelength-wise error (Linear and Second degree polynomial fit via LS) for Nokia 1520 in testing the influence of JPEG compression in reflectance estimation (spatial non-homogenous case)

Figure 26 and Table 10 show that there is a clear difference spectrally between the estimated spectra obtained from the RAW images and the one obtained from the JPEG images. We see that the lowest RMSE errors (and highest GFC values) come from using the RAW images and then they increase by increasing the compression

ratio in the JPEG images, thus making the recovered spectra from the JPEG image with 50% quality having the highest error. The result doesn't change when a different recovery methods of the spectra is used, namely the second degree polynomial fitting.

Table 9 showing the CIELAB and CIEDE2000 color differences present similar results as obtained previously in the sense that there is difference between the estimation done with the RAW and estimation done with JPEG. What is more interesting now is the level of color difference. Previously the color difference, when comparing RAW and JPEG, was quite small, but now we see that it increases exponentially. According to Abrado et al. [48] the results with CIELAB color difference smaller than 10 is considered sufficient. In our case we see that the mean color differences when using JPEG 75% and 50% quality are above this threshold. The only mean color difference smaller than 10 CIELAB units was obtained from the RAW and JPEG 100% quality images. This fact stands true independent of the type of estimation method employed.

Table 9 CIELAB and CIEDE2000 color differences (Linear and Second degree polynomial fit via LS) for Nokia 1520 in testing the influence of JPEG compression in reflectance estimation (spatial non-homogenous case)

		CIELAB				CIEDE2000			
		Min	Mean	Max	Standard deviation	Min	Mean	Max	Standard deviation
Liniar fit	Nokia 1520 raw	0.3	3.9	12.5	2.5	0.4	2.5	8.7	1.4
	Nokia 1520 JPEG100%	0.9	8.7	31.5	5.6	0.7	4.5	14.1	2.1
	Nokia 1520 JPEG 75%	1.8	13.3	43.0	8.7	1.2	6.5	16.1	3.0
	Nokia 1520 JPEG 50%	1.5	15.2	56.0	10.6	1.1	7.5	17.5	3.7
Second degree polynomial fit	Nokia 1520 raw	0.7	2.8	10.5	1.8	0.5	1.7	4.7	0.8
	Nokia 1520 JPEG100%	0.8	7.8	33.8	5.4	0.8	3.9	10.8	1.9
	Nokia 1520 JPEG 75%	1.6	12.8	43.7	8.6	1.3	6.2	15.9	2.8
	Nokia 1520 JPEG 50%	1.1	14.5	56.0	10.6	0.8	7.0	18.1	3.8

Table 10 RMSE and GFC errors(Linear and Second degree polynomial fit via LS) for Nokia 1520 in testing the influence of JPEG compression in reflectance estimation (spatial non-homogenous case)

		RMSE				GFC			
		Min	Mean	Max	Standard deviation	Min	Mean	Max	Standard deviation
Linear fitting	Nokia 1520 raw	0.014	0.043	0.114	0.018	0.798	0.978	0.999	0.035
	Nokia 1520 JPEG 100%	0.016	0.051	0.143	0.023	0.839	0.977	0.999	0.032
	Nokia 1520 JPEG 75%	0.023	0.060	0.168	0.027	0.810	0.969	0.999	0.038
	Nokia 1520 JPEG 50%	0.0193	0.064	0.164	0.029	0.768	0.966	0.999	0.040
Second degree polynomial fitting	Nokia 1520 raw	0.007	0.038	0.083	0.017	0.816	0.984	0.999	0.026
	Nokia 1520 JPEG 100%	0.012	0.046	0.129	0.022	0.867	0.984	0.999	0.023
	Nokia 1520 JPEG 75%	0.011	0.056	0.158	0.027	0.861	0.976	0.999	0.029
	Nokia 1520 JPEG 50%	0.011	0.060	0.160	0.029	0.767	0.972	0.999	0.036

5.1.3 Conclusion

This experiment has shown that, as expected, JPEG type compression plays an important role in obtaining the spectral data, namely that it provides worse approximations than the estimations obtained from the RAW data. This statement is true for all the devices where the RAW data was available.

However it is possible to obtain somewhat close approximations to the estimations obtained from the RAW data when considering high level quality JPEG image. Still,

special attention is needed when the imaged objects are not represented in a homogenous type space, but as a real case scenario in which they contain high level of detail.

5.2 Testing how the image processing block in digital image affects reflectance estimation in smartphones

Another important step in investigating the value of the smartphone as a pocket spectral imaging device was to test how the image processing block affects reflectance estimation in comparison with the RAW images.

In order to test this we considered the JPEG and RAW images with the Xrite Color Checker Digital SG taken with all the devices. The images were used further in recovery of the spectral data. Again the estimation methods used were liniar fitting via least squares and polynomial fitting via least squares. The evaluation was anew LOO.

As we saw previously that compression plays an important role in spectral data recovery, we tried eliminating these effects for the cases when JPEG type data was used. This was done by choosing the highest quality images that were possible to obtain from the smartphones and digital cameras and also by considering for estimation the case where the samples are spatially homogenous.

5.2.1 Liniar fitting via least squares

Results can be seen in Figure 27 and Tables 11, 12 for liniar fitting. Firstly we see from Figure 27 that estimation errors obtained from JPEG are much higher than the ones obtained from the RAW. Secondly we notice that estimating the reflectance from RAW images provides the most stable results, as RMSE wavelength errors are closely grouped together, while the ones obtained from the JPEG images vary considerably in shape and intensity. Thirdly we see that from JPEG type outputs the lowest error comes from the Iphone device while the highest one comes from the Nikon D800 camera.

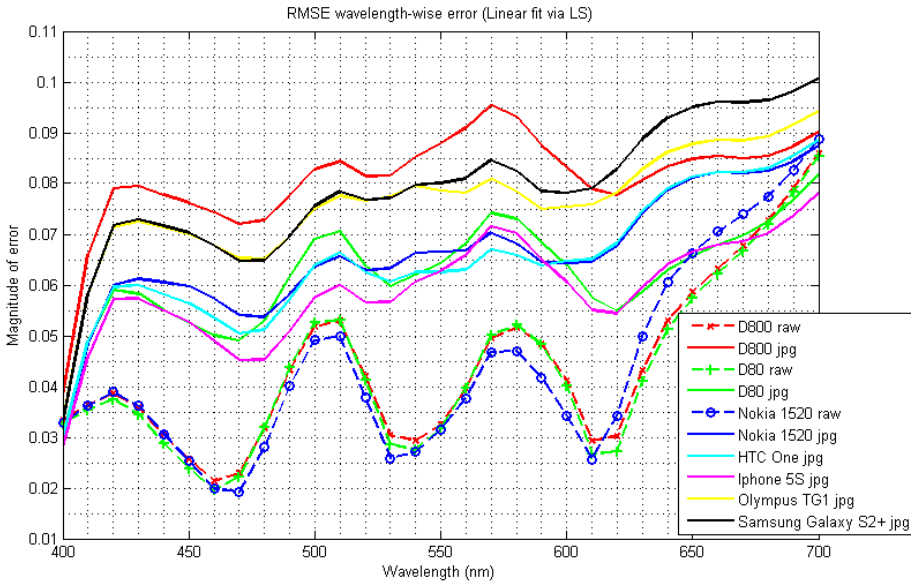

Figure 27 RMSE wavelength-wise error (Linear fit via LS) for all devices in testing the influence of image processing block in reflectance estimation

From Table 11 we see that from a colorimetric point of view the results obtained from JPEG are quite bad when using liniar fitting. The mean CIELAB color differences for all the devices where JPEG was considered was higher than when RAW images were used, having values ranging between 15 and 25.This makes the reconstructed spectra unusable from the color point of view according to Abrado et al. [48]

Table 11 CIELAB and CIEDE2000 color differences (Linear fit via LS) for all devices in testing the influence of image processing block in reflectance estimation

	CIELAB				CIEDE2000			
	Min	Mean	Max	Standard deviation	Min	Mean	Max	Standard deviation
D800 raw	0.3	3.9	12.5	2.5	0.4	2.5	8.7	1.4
D800JPEG	1.7	29.1	158.9	35.1	2.0	11.9	42.6	11.1
D80 RAW	0.5	3.7	11.0	2.3	0.3	2.4	7.9	1.3
D80 JPEG	1.1	16.0	58.9	14.8	1.3	7.8	31.5	6.8
Nokia RAW	0.5	4.1	11.6	2.5	0.3	2.6	11.6	1.9

Nokia JPEG	1.7	20.6	90.8	22.2	1.7	9.0	36.5	7.7
HTC JPEG	2.1	16.1	69.0	16.3	1.4	8.3	34.7	7.7
IPHONE JPEG	0.9	15.5	80.2	17.6	0.8	7.2	30.7	6.8
OLYMPUS JPEG	2.2	24.0	102.6	24.3	2.1	10.7	40.1	9.2
SAMSUNG JPEG	2.3	21.3	102.5	23.7	1.8	10.0	40.1	9.1

Considering the spectral metrics RMSE and GFC we remark from Table 12 that we can infer the same information as from the color difference table. Thus we see again that RMSE values are lower for estimations obtained from the RAW images, while estimations from JPEG images are higher. The mean GFC values are all lower than 0.995 which is considered the basic necessary for acceptable estimation results. This is caused due to the simplistic method used in estimation, but also because of the devices themselves as they were not conceived with reflectance recovery purpose in mind.

Table 12 RMSE and GFC errors (Linear fit via LS) for all devices in testing the influence of image processing block in reflectance estimation

	RMSE				GFC			
	Min	Mean	Max	Standard deviation	Min	Mean	Max	Standard deviation
D800 raw	0.014	0.043	0.114	0.018	0.798	0.978	0.999	0.035
D800JPEG	0.025	0.075	0.264	0.030	0.020	0.938	0.999	0.151
D80 RAW	0.014	0.042	0.115	0.018	0.786	0.977	0.999	0.036
D80 JPEG	0.024	0.058	0.205	0.023	0.040	0.931	0.999	0.179
Nokia RAW	0.008	0.042	0.149	0.022	0.718	0.976	0.999	0.041
Nokia JPEG	0.029	0.063	0.178	0.022	0.051	0.930	0.999	0.186
HTC JPEG	0.025	0.062	0.179	0.023	0.303	0.940	0.999	0.144
IPHONE	0.017	0.055	0.185	0.023	0.043	0.932	0.999	0.188

JPEG								
OLYMPUS JPEG	0.028	0.072	0.237	0.026	0.042	0.942	0.998	0.146
SAMSUNG JPEG	0.030	0.074	0.258279	0.029	0.026	0.934	0.999	0.172

5.2.2 Second degree polynomial fitting via least squares

When applying the Second degree polynomial estimation method the results change. Figure 28 containing the RMSE wavelength-wise error doesn't show anymore the high discrepancy that we saw before in liniar fitting between RAW and JPEG images. Visually now we see that the lowest errors corresponds still to RAW data from Nokia 1520. Numerically however we see from Table 14 that the mean values corresponding to the lowest spectral errors correspond to JPEG type data coming mainly from smartphone type devices such as Iphone, HTC, Nokia, but also the commercial Olympus digital camera. GFC values, although under the limit of what can be considered as a good reconstruction, also puts Nokia and IPhone as the devices with the best reconstructed spectra compared with the raw data obtained from DSLR cameras.

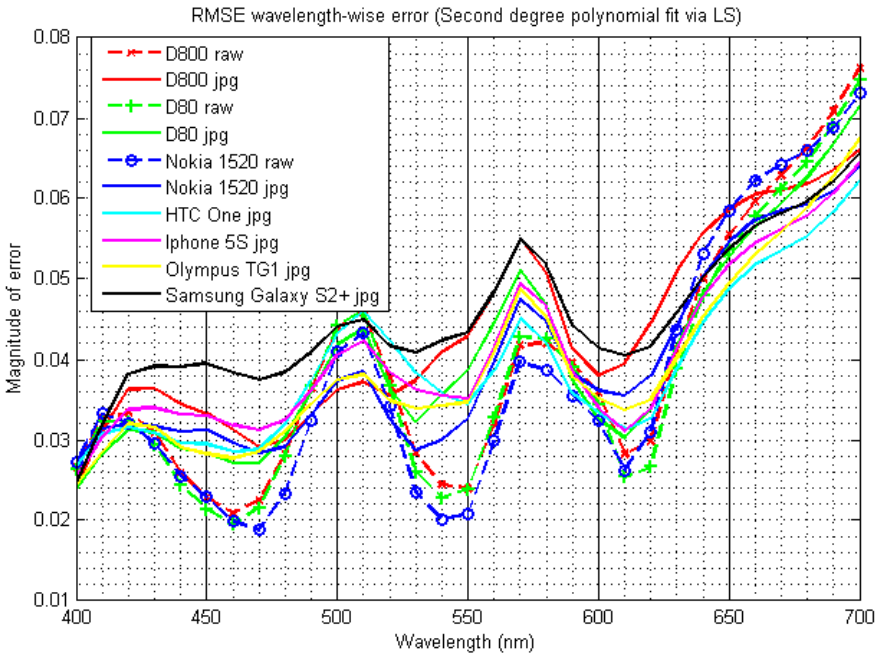

Figure 28 RMSE wavelength-wise error (Second degree polynomial fit via LS) for all devices in testing the influence of image processing block in reflectance estimation

Table 13 paints another picture of the results than Table 14. While spectrally the recovered data is best when using the mobile cameras, from a color difference point of view results show that still devices which can obtain the RAW data provide lower color difference values. Still the values obtained for the mobile devices are all under the 6 CIELAB color difference scale. Obtaining color difference values under 6 CIELAB units considered the estimated spectra as being of good quality by Abrado et al [48].

Table 13 CIELAB and CIEDE2000 color differences (Second degree polynomial fit via LS) for all devices in testing the influence of image processing block in reflectance estimation

	CIELAB				CIEDE2000			
	Min	Mean	Max	Standard deviation	Min	Mean	Max	Standard deviation
D800 raw	0.5	2.8	10.4	1.8	0.4	1.7	4.7	0.8
D800JPEG	0.3	6.4	27.3	4.8	0.1	3.7	13.9	2.8
D80 RAW	0.2	2.8	8.1	1.7	0.2	1.7	4.1	0.8
D80 JPEG	0.9	5.3	19.1	4.0	0.3	3.2	15.5	2.7
Nokia RAW	0.5	3.7	10.7	2.3	0.3	2.1	6.5	1.1
Nokia JPEG	0.4	4.1	11.3	2.4	0.4	2.6	8.5	1.5
HTC JPEG	0.9	5.4	16.9	3.6	0.9	3.6	15.4	2.5
IPHONE JPEG	0.4	4.0	16.4	2.9	0.2	2.5	7.1	1.4
OLYMPUS JPEG	0.9	5.6	18.1	3.7	0.6	3.4	14.2	2.7
SAMSUNG JPEG	0.9	7.1	28.9	4.5	0.3	4.4	16.6	3.1

Table 14 RMSE and GFC errors (Second degree polynomial fit via LS) for all devices in testing the influence of image processing block in reflectance estimation

	RMSE				GFC			
	Min	Mean	Max	Standard deviation	Min	Mean	Max	Standard deviation
D800 raw	0.007	0.038	0.083	0.017	0.815	0.984	0.999	0.026
D800JPEG	0.015	0.039	0.117	0.021	0.895	0.989	0.999	0.017
D80 RAW	0.007	0.037	0.083	0.016	0.816	0.984	0.999	0.027
D80 JPEG	0.009	0.037	0.115	0.020	0.851	0.986	0.999	0.025
Nokia RAW	0.007	0.036	0.119	0.018	0.771	0.984	0.999	0.029
Nokia JPEG	0.007	0.036	0.099	0.020	0.902	0.990	0.999	0.015
HTC JPEG	0.006	0.035	0.094	0.019	0.905	0.989	0.999	0.020
IPHONE JPEG	0.010	0.036	0.114	0.020	0.891	0.991	0.999	0.015
OLYMPUS JPEG	0.004	0.036	0.113	0.018	0.868	0.989	0.999	0.021
SAMSUNG JPEG	0.009	0.040	0.144	0.021	0.852	0.987	0.999	0.023

5.2.3 Conclusion

We saw in this test that even though we tried to reduce the effect of JPEG type compression, it still played an important role when testing the influence of the image processing block in reflectance estimation. This happened for all the devices considered be they mobile cameras or DSLR cameras.

Another point that was seen here was that dependent on the estimation method used, there is the possibility that under certain conditions, the estimation obtained from smartphone cameras is better from a spectral point of view than the estimation obtained from raw data of DSLR cameras. However colorimetric error values are still higher. We noticed thus that the CIELAB errors are not statistically consistent with the spectral errors. This is caused by the fact that we have a nonlinear transform from the spectral reflectance to CIELAB values, thus the solution obtained as estimated spectra is not optimal when evaluated by colorimetric error [27].

5.3 Testing how smartphone cameras perform in reflectance estimation when considering natural materials

For this test the natural materials chart presented in Chapter 4 was used for estimation. The chart was imaged by all the devices and the RGB images were used similarly in estimation methods. These include liniar fitting, second degree polynomial fitting, and third-degree polynomial fitting.

In this case however, the natural materials chart was used just as test data, while for training the 96 samples of the Xrite Color Checker Digital SG was used.

5.3.1 Liniar fitting via least squares

Results for liniar fitting are shown in Figure 29 and Tables15, 16.

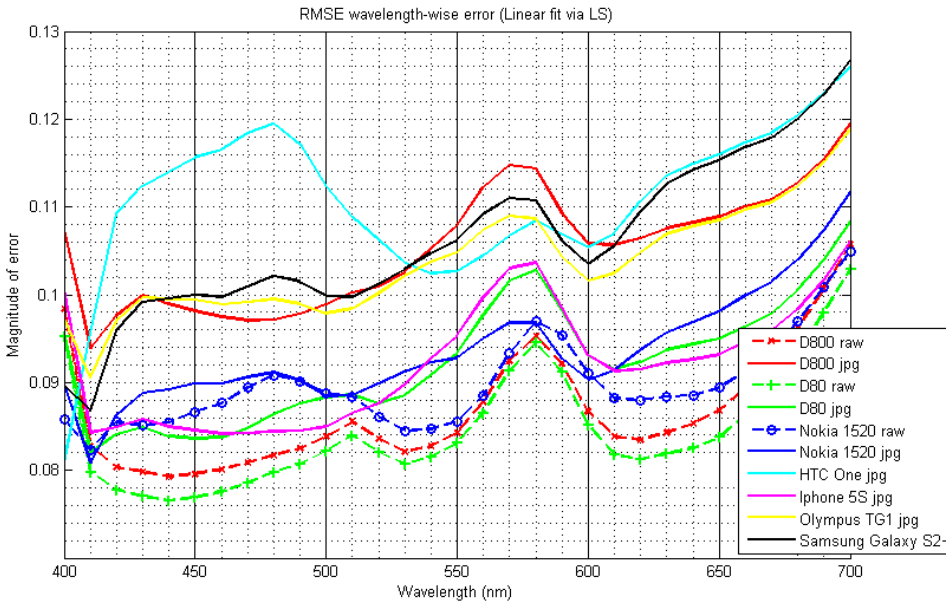

Figure 29 RMSE wavelength-wise error (Linear fit via LS) for all devices in testing the performance of mobile cameras in reflectance estimation using a natural materials chart

Figure 29 presents the RMSE wavelength-wise errors. As seen before in the image processing block testing the lowest errors are obtained from the RAW data for Nikon D800, Nikon D80 and Nokia 1520 devices (with some variation in the blue region between the Nokia 1520 and Nikon cameras). This variation it is caused due to the high level of noise present in the RAW Nokia 1520 image.

Still low errors results from JPEG data are obtained for Iphone and Nokia type devices. These statements stand true when considering error measures both spectrally and colorimetrically as it can be seen in Tables 15 and 16.

Furthermore Figure 29 and Tables 15, 16 also show that the worst estimations come from devices such as Samsung, Olympus with the worst being HTC device.

Table 15 CIELAB and CIEDE2000 color differences (Linear fit via LS) for all devices in testing the performance of mobile cameras in reflectance estimation using a natural materials chart

	CIELAB				CIEDE2000			
	Min	Mean	Max	Standard deviation	Min	Mean	Max	Standard deviation
D800 raw	0.9	5.9	34.5	5.2	0.5	4.7	24.0	3.5
D800JPEG	0.3	16.8	118.1	23.4	0.4	9.5	53.6	10.0
D80 RAW	0.5	5.9	33.3	5.0	0.5	4.8	23.1	3.4
D80 JPEG	2.0	10.5	59.1	9.9	1.5	7.1	35.2	5.7
Nokia RAW	1.5	7.5	35.3	5.6	1.2	5.7	24.4	3.5
Nokia JPEG	0.9	9.8	39.7	7.0	0.8	7.1	25.0	4.1
HTC JPEG	3.0	11.9	40.9	6.7	3.1	8.7	19.3	3.6
IPHONE JPEG	1.5	9.5	63.3	9.6	1.3	6.8	34.2	5.6
OLYMPUS JPEG	1.6	11.9	76.8	10.3	1.0	8.2	38.8	5.5
SAMSUNG JPEG	0.8	10.8	56.3	7.1	0.9	7.7	27.4	3.7

Table 16 RMSE and GFC errors (Linear fit via LS) for all devices in testing the performance of mobile cameras in reflectance estimation using a natural materials chart

	RMSE				GFC			
	Min	Mean	Max	Standard deviation	Min	Mean	Max	Standard deviation
D800 raw	0.014	0.059	0.598	0.063	0.701	0.980	0.999	0.049
D800JPEG	0.016	0.081	0.540	0.067	0.322	0.942	0.999	0.142
D80 RAW	0.016	0.059	0.586	0.060	0.699	0.980	0.999	0.048
D80 JPEG	0.017	0.072	0.530	0.057	0.255	0.957	0.999	0.125

Nokia RAW	0.013	0.071	0.522	0.054	0.767	0.982	0.999	0.040
Nokia JPEG	0.012	0.075	0.503	0.056	0.575	0.978	0.999	0.054
HTC JPEG	0.023	0.096	0.457	0.054	0.824	0.982	0.999	0.031
IPHONE JPEG	0.020	0.069	0.546	0.061	0.124	0.960	0.999	0.131
OLYMPUS JPEG	0.015	0.083	0.535	0.061	0.481	0.968	0.999	0.084
SAMSUNG JPEG	0.015	0.089	0.456	0.057	0.615	0.976	0.999	0.057

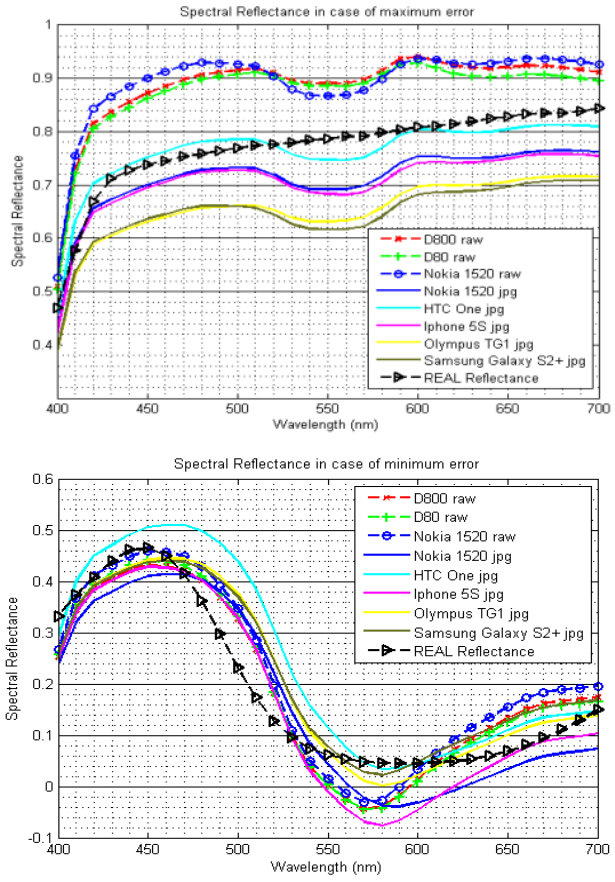

Figure 30 Estimated Spectral reflectance for maximum and minimum spectral error respectively (Linear fit via LS) for all devices in testing the performance of mobile cameras in reflectance estimation using a natural materials chart

It is important to acknowledge here the fact that largest errors appeared due to the natural samples used. As previously stated, the chart was not build with the goal of testing color accuracy or reflectance estimation through different devices. Therefore it contains rough samples, with different thicknesses, transparencies, and reflectivity. The highest errors obtained involved materials that belonged to plastics category (such as transparent plastics) or metal category (such as aluminium foil), while the lowest errors came from the paper and carton category. Figure 30 shows the estimated spectral reflectance for the maximum error in the case of aluminium samples and the minimum error in the case of a paper sample.

5.3.2 Second degree polynomial fitting via least squares

Results for Second degree polynomial fitting are shown in Figure 31 and Tables 17, 18.

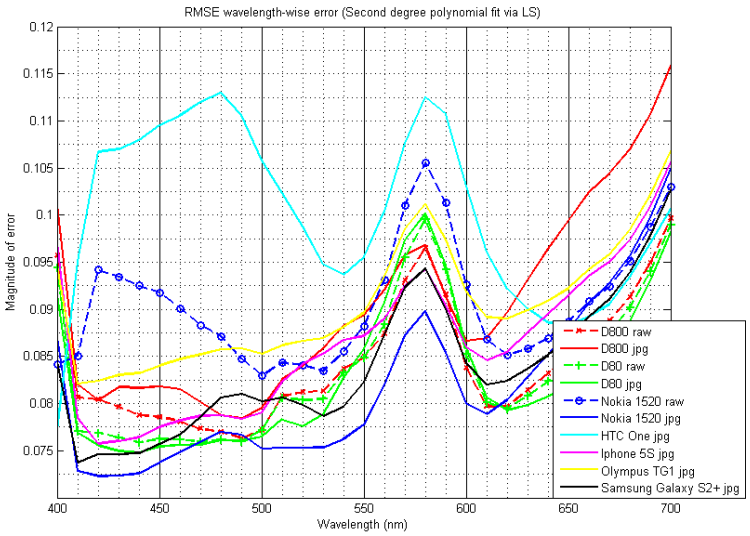

Figure 31 RMSE wavelength-wise error (Second degree polynomial fit via LS) for all devices in testing the performance of mobile cameras in reflectance estimation using a natural materials chart

Figure 31 presents the RMSE wavelength-wise errors for the Second degree polynomial fitting. Here we see immediately that the lowest RMSE wavelength-wise error corresponds to the estimation where Nikon 1520 JPEG is used followed by that of the Iphone device. Numerically we can also infer the same from Table 18, which shows JPEG data from Nikon and Iphone provides the lowest RMSE errors (and highest GFC values). Furthermore we notice from Figure 31 that, what was a slight variation in the error curves (in the blue region) obtained from the Nokia 1520 and the Nikon cameras, now it has become quite big due to the exponential increase of the error caused by the polynomial estimation.

Similar to the liniar fitting method the highest RMSE estimation error comes from the JPEG data of HTC device.

Furthermore from Table 18 we can ascertain that even though the smallest spectral errors were obtained from smartphones like Iphone and Nokia, color differences are smaller when using the RAW data from Nikon D800 and Nikon D80 devices.

Table 17 CIELAB and CIEDE2000 color differences (Second degree polynomial fit via LS) for all devices in testing the performance of mobile cameras in reflectance estimation using a natural materials chart

	CIELAB				CIEDE2000			
	Min	Mean	Max	Standard deviation	Min	Mean	Max	Standard deviation
D800 raw	0.8	5.4	33.1	4.6	0.7	4.1	22.8	3.0
D800JPEG	0.7	7.2	39.3	6.3	0.8	5.2	23.5	3.8
D80 RAW	0.6	5.4	31.8	4.7	0.5	4.2	21.8	3.12
D80 JPEG	1.1	6.5	39.4	5.5	0.6	4.5	21.5	3.1
Nokia RAW	0.9	7.5	30.0	4.7	0.5	5.8	19.6	2.9
Nokia JPEG	1.8	6.1	30.8	4.8	1.1	4.7	21.2	2.9
HTC JPEG	1.9	9.1	28.9	5.1	1.7	6.9	22.7	3.5
IPHONE JPEG	1.0	6.0	34.3	5.2	0.8	4.5	23.9	3.3
OLYMPUS JPEG	1.0	6.5	38.2	6.0	1.1	5.0	23.9	3.8
SAMSUNG JPEG	1.2	7.1	32.5	5.1	0.9	5.0	25.1	3.5

Table 18 RMSE and GFC errors (Second degree polynomial fit via LS) for all devices in testing the performance of mobile cameras in reflectance estimation using a natural materials chart

	RMSE				GFC			
	Min	Mean	Max	Standard deviation	Min	Mean	Max	Standard deviation
D800 raw	0.012	0.058	0.584	0.061	0.745	0.984	0.999	0.038
D800JPEG	0.00	0.063	0.596	0.065	0.740	0.984	0.999	0.037

D80 RAW	0.010	0.058	0.571	0.060	0.758	0.983	0.999	0.038
D80 JPEG	0.009	0.058	0.565	0.059	0.759	0.985	0.999	0.034
Nokia RAW	0.021	0.071	0.527	0.055	0.820	0.985	0.999	0.030
Nokia JPEG	0.010	0.056	0.551	0.060	0.862	0.988	0.999	0.024
HTC JPEG	0.020	0.081	0.498	0.059	0.860	0.987	0.999	0.023
IPHONE JPEG	0.008	0.057	0.594	0.065	0.833	0.986	0.999	0.029
OLYMPUS JPEG	0.010	0.060	0.598475	0.068	0.768	0.986	0.999	0.033
SAMSUNG JPEG	0.009	0.063	0.488	0.055	0.788	0.986	0.999	0.028

5.3.3 Third degree polynomial fitting via least squares

Connah et al suggests in his paper [28] that increasing the degree of the polynomial in the reflectance recovery method improves the results and lowers the estimation errors. For this test case scenario we went a step further and have done the estimation using the third grade polynomial method via least squares fit.

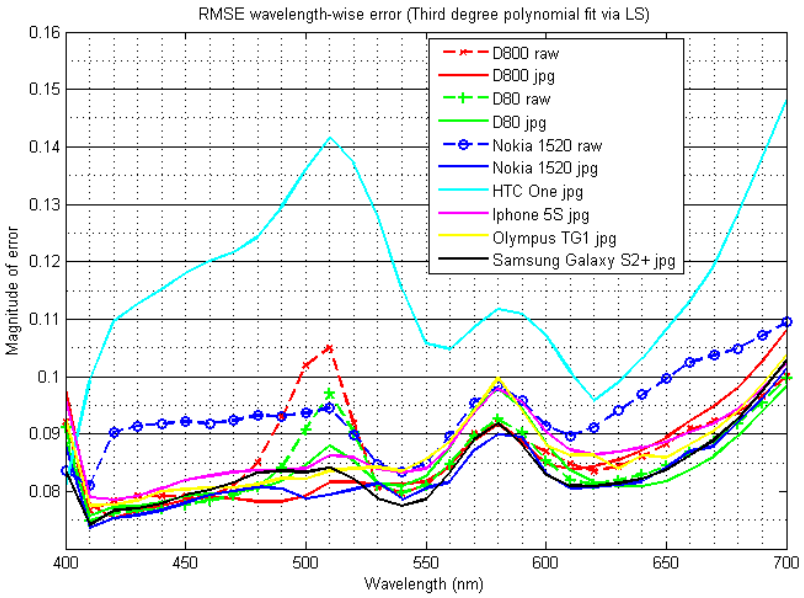

Figure 32 RMSE wavelength-wise errors (Third degree polynomial fit via LS) for all devices in testing the performance of mobile cameras in reflectance estimation using a natural materials chart

When using this estimation method, results are similar to the ones obtained in the second degree polynomial fitting case. Therefore we see that spectrally the lowest error measure corresponds to devices such as Iphone, Nokia 1520 and Nikon D800 where JPEG data is used (Table 20). GFC values also points to the same scenario where Iphone and Nokia 1520 obtain the best results by having the highest GFC values. Visually we see from Figure 33 that the third degree polynomial smoothes out the errors in cases where JPEG data is used for estimation, whereas the cases where RAW data is used, it smoothes out the errors only in the region where sensor has sensitivity. In the regions where the sensor is less sensitive such as the regions where we have the intersection of channels sensitivity (at 510nm and 570nm) we notice high peaks of spectral errors.

As we already got accustomed the results shows that colorimetrically the lowest color differences are obtained by estimations that used the RAW camera data (Table 19). Color differences for smartphone devices have means lower than 10 which makes them acceptable by Abrado et al.

Table 19 CIELAB and CIEDE2000 color differences (Second degree polynomial fit via LS) for all devices in testing the performance of mobile cameras in reflectance estimation using a natural materials chart

	CIELAB				CIEDE2000			
	Min	Mean	Max	Standard deviation	Min	Mean	Max	Standard deviation
D800 raw	0.7	5.3	33.7	4.7	0.6	4.1	23.3	3.1
D800JPEG	0.6	5.1	34.3	4.9	0.4	3.9	23.8	3.3
D80 RAW	0.8	5.3	32.7	4.5	0.8	4.0	22.5	3.1
D80 JPEG	1.1	6.0	35.1	5.1	0.8	4.3	21.9	3.0
Nokia RAW	1.4	7.7	33.2	4.9	0.7	5.8	19.8	3.2
Nokia JPEG	0.7	7.0	36.3	5.5	0.4	5.1	22.0	3.2
HTC JPEG	3.0	11.3	45.9	8.0	3.0	8.2	21.9	4.4
IPHONE JPEG	0.7	5.8	34.3	5.2	0.5	4.4	23.8	3.6
OLYMPUS JPEG	0.6	6.4	33.6	5.2	0.6	5.3	23.2	3.6
SAMSUNG JPEG	1.6	7.0	32.0	4.8	1.0	5.4	23.7	3.4

Table 20 RMSE and GFC errors for (Second degree polynomial fit via LS) for all devices in testing the performance of mobile cameras in reflectance estimation using a natural materials chart

	RMSE				GFC			
	Min	Mean	Max	Standard deviation	Min	Mean	Max	Standard deviation
D800 raw	0.011	0.059	0.588	0.064	0.821	0.986	0.999	0.029
D800JPEG	0.006	0.055	0.598	0.066	0.846	0.989	0.999	0.023
D80 RAW	0.009	0.058	0.578	0.062	0.833	0.987	0.999	0.027
D80 JPEG	0.008	0.059	0.569	0.060	0.843	0.988	0.999	0.026
Nokia RAW	0.020	0.073	0.527	0.058	0.838	0.988	0.999	0.025
Nokia JPEG	0.008	0.055	0.559	0.061	0.876	0.989	0.999	0.019
HTC JPEG	0.022	0.091	0.503	0.072	0.728	0.980	0.999	0.038
IPHONE JPEG	0.006	0.056	0.592	0.067	0.844	0.988	0.999	0.024
OLYMPUS JPEG	0.011	0.058	0.589	0.064	0.856	0.987	0.999	0.026
SAMSUNG JPEG	0.008	0.063	0.507	0.055	0.870	0.988	0.999	0.023

5.3.4 Conclusion

In this last experiment we tested the performance of current smartphone cameras in terms of reflectance estimation in the case where the imaged data is represented by natural materials. Results have shown that under certain conditions currently there are mobile cameras that can perform similarly or even outperform DSLR cameras spectrally.

6 Conclusions and Future Work

In this work we focused on studying the practicality and usefulness of smartphones and their cameras as a single standing spectral imaging device. The study in the thesis is structured as a comparison between smart-phone cameras and DSLR cameras as their digital output in the form of RAW (obtained mainly from the DSLR cameras) and JPEG type data provide an important role in obtaining the spectral estimation of the imaged objects. Several test cases were made in order to see the problems that arise when considering smartphone devices as spectral imaging devices. Upon recovering the spectral data diffrent reflectance estimation methods were implemented such as the liniar fitting via least square and multivariate polynomial fitting via least squares. Also evaluation of the estimation methods were realized by implementing different spectral and colorimetric metrics such as RMSE, GFC and RMSE wavelength-wise, CIELAB and CIEDE2000 color differences.

The problems considered were how the JPEG type compression algorithm and also how the image processing block influences reflectance recovery. This experiment has shown that, as expected, JPEG type compression plays an important role in obtaining the spectral data, namely that it provides worse estimations with increasing level of compression than the estimations obtained from the RAW data. However under the tested conditions it is possible to obtain somewhat close reflectance estimations (to the ones obtained from the RAW data) when considering using high level quality JPEG image. Similarly it was found that the image processing block plays also quite an important role influencing a great deal the estimation. Results showed that even though smartphone cameras have similar type of sensors recovery accuracy varies greatly between devices.

Also performance of current smartphone cameras in terms of reflectance estimation was tested in the case where the imaged data is represented by natural materials. Results have shown that under certain conditions, currently there are mobile cameras such as Nokia 1520 and Iphone 5S that can offer spectral recovery similarly to DSLR cameras even with JPEG type formats. However RAW data from DSLRs offers more “stable” results colorimetrically. This statistical inconsistency is caused by the fact that we have a nonlinear transform from the spectral reflectance to CIELAB values, thus the solution obtained as estimated spectra is not optimal when evaluated by colorimetric error.

Another aspect found when trying to use the smartphone as a spectral imaging device is that it emplies the usage of certain estimation models. This is due to the inability of the user to have access to the sensitivities of the sensor (due to company policies, and inability to capture RAW data), which represents much needed information in many recovery methods. Thus we have a limitation of the estimation models that can be employed.

Future work involves testing the reflectance recovery when using as training, charts with more color samples. It is widely known in literature that increasing the number

of training samples the accuracy in spectral recovery will be greater improved. Also it would be interesting to see what is the minimum number of training samples in order to obtain good spectral data from the smartphones. Also as future work it is needed to see how different illumination and estimation methods affects the results obtained so far.

Even more the final goal is to create custom software application which includes reduced and adapted image processing in order provide analytical measurements of a spectral image. This can be used in a broad range of fields such as it will allow a novice user to use applications that carry out analysis on objects that require spectral information mobile imaging in artworks, cultural heritage, medical imaging, pattern recognition (automated photo editing) etc.

Bibliography

[1] Koskinen I.K., 2007, *Mobile Multimedia in Action*, by Transaction Publishers, New Brunswick, New Jersey.

[2] Kindberg, T., Spasojevic, M., Fleck, R. & Sellen, A., 2005, *The ubiquitous camera: an in-depth study of camera phone use'*, in IEEE Pervasive Computing, vol. 4, no. 2, Apr.– Jun.

[3] Gye L. 2007, *Picture This: The Impact of Mobile Camera Phones on Personal Photographic Practices*, published in Continuum Vol 21 Issue 2. pp 279-288

[4] Slavuj R., Green P., *To develop a method for estimating spectral reflectance from camera RGB values*, The Norwegian Color and Visual Computing Laboratory, Gjøvik, Norway

[5] Hardeberg J. Y., Schmitt F., and Brettel. H., 2002, *Multispectral color image capture using a liquid crystal tunable filter*. Optical Engineering, 41

[6] Berns R. S., Taplin L. A., Nezamabadi M., Mohammadi M., and Zhao Y., 2005, *Spectral imaging using a commercial colorfilter array digital camera*. In 14th Triennal ICOM-CC meeting, pages 743–750

[7] Hyvarinen T., Herrala E., Dall'Ava A., 1998, *Direct sight imaging spectrograph: a unique add-on component brings spectral imaging to industrial applications*, Proc. SPIE

[8] Hirai A., Hashimoto M., Itoh K. and Ichioba Y., 1997, *Multichannel spectral imaging system for measurement with high signal-to-noise ratio*, Optical Review 4, 334-341

[9] Heikkinen V., Mirhashemi A., Alho J., 2013, *Link functions and Matérn kernel in the estimation of reflectance spectra from RGB responses*, J. Opt. Soc. Am. A / Vol. 30, No. 11 / November 2013

[10] Jiang J., Gu J., 2012, *Recovering Spectral Reflectance under commonly lighting conditions*, Computer Vision and Pattern Recognition Workshops (CVPRW)

[11] Imai F., Berns R. S., and Tzeng D., 2000, *A comparative analysis of spectral reflectance estimation in various spaces using a trichromatic camera system*, J. Imaging Sci. Technol. 44, 280–287

[12] Gebejes A., Martinez Domingo M. A., Heikkinen V., Tomic I., Sept 2013, *Reflectance recovery for coated printed color samples via multiangular RGB camera measurements*, , Color and Visual Computing Symposium

[13] Miya., Miyata K, 1999, *Color Image Processing Based on Spectral Information and Its Application*, Image Processing, ICIP 99. Proceedings

[14] Stigell P., Miyata K., Hauta-Kasari M., 2007, *Wiener Estimation Method in Estimating of Spectral Reflectance from RGB Images*, ISSN 1054-6618, Pattern Recognition and Image Analysis, 2007, Vol. 17, No. 2, pp. 233–242. © Pleiades Publishing, Ltd.,

[15] Hae Song J., Kim C., Yoo Y., March 2014, *Vein Visualization using a Smart Phone with Multispectral Wiener Estimation for Point-of-Care Applications*, published in Biomedical and Health Informatics, IEEE Journal of (Volume:PP , Issue: 99),

[16] Ohta N. and Robertson A. R., 2005, *Colorimetry. Fundamentals and Applications*, John Wiley & Sons, Ltd

[17] Fairchild M. D., Rosen M. R., Johnson G. M., *Spectral and Metameric Color Imaging Technical Report*, Munsell Color Science Laboratory

[18] Gebejes A., Tomic I., Karlovic I. and Juric I., 2012, *Evaluation of the algorithms for recovering spectral reflectance from virtual digital camera response*, Journal of Graphic Engineering and Design

[19] Electro Magnetic Spectrum, [Online]. Available: http://www.pion.cz/en/article/electromagnetic-spectrum

[20] Digital Camera Signal Processing Flow, [Online]. Available: http://panasonic.jp/support/global/cs/dsc/knowhow/knowhow30.html

[21] Huang B-C., Fuh C-S., 2005, *Image Pipeline Algorithms for Standard Mobile Imaging Architecture Sensors*, 18th IPPR Conference on Computer Vision, Graphics and Image Processing (CVGIP 2005)

[22] Chen T., 2003, *Digital Camera System Simulator and Applications*, Phd Thesis

[23] Nakamura J., 2006, *Image Sensors and Signal Processing for Digital Still Cameras*, published by CRC press, Taylor & Francis Group

[24] Zhou P., 2007, *Getting the Most out of Your Image-Processing Pipeline*, white paper of Texas Instruments Incorporated

[25] Lebourgeois V., Begue A., Labbe S., Mallavan B., Prevot L. and Roux B. , 2008, *Can Commercial Digital Cameras Be Used as Multispectral Sensors? A Crop Monitoring Test, Sensors*, 8, 7300-7322; DOI: 10.3390/s8117300

[26] Shimano N., Terai K., Hironaga M., October 2007, *Recovery of spectral reflectances of objects being imaged by multispectral cameras*, Vol. 24, No.10, Journal Opt. Soc. Am. A

[27] Zhang W.F., Dai D.Q., September 2008, *Spectral reflectance estimation from camera responses by support vector regression and a composite model,* J. Opt. Soc. Am , A/Vol. 25, No. 9/ Sept. 2008

[28] Connah D., Hardeberg J. Y., 2005, *Spectral recovery using polynomial models*, Proc. SPIE 5667, 65-75

[29] Heikkinen V., Lenz R., Jestsu T., Parkkinen J., Hauta-Kasari M., Jaaskelainen T., October 2008, *Evaluation and unification of some methods for estimating reflectance spectra from RGB images*, J. Opt. Soc. Am. A/Vol. 25, No. 10/

[30]Heikkinen V., Jestu T., Parkkinen J., Hauta-Kasari M., Jaaskelainen T. and Lee S. D., 2007, *Regularized learning framework in the estimation of reflectance spectra from camera responses*, J. Opt. Soc. Am. A 24, 2673-2683

[31] Hardeberg J. Y, 2004, *Filter selection for multispectral color image acquisition*, J. Imaging Sci. Technol., 48, 105-110

[32] Nieves J. L., Valero E. M., Nascimento S. M. C., Andres J. H., and Romero J., 2005, *Multispectral synthesis of daylight using a commercial digital CCD camera*, Appl . Opt., 44, 5696-5703

[33] Jetsu T., Heikkinen V., Parkkinen J., Hauta-Kasari M., Martinkauppi B., Lee S. D., Ok H. W. and Kim C. Y., 2006, *Color calibration of digital camera using polynomial transformation*, in CGIV, Third European Conference on Color Graphics, Imaging and Vision (IS&T,), 163-166

[34] Haneishi H., Hasegawa T., Hosoi A., Yokoyama Y., Tsumura N. and Miyake Y., 2000, *System design for accurately estimating the reflectance spectra of art paintings*, Appl. Opt., 39, 6621-6623 ()

[35] Hernandez-Andres J., Romero J., Garcıa-Beltran A., and Nieves J.L., 1998, *Testing linear models on spectral daylight measurements*, Appl. Opt. 37, 971–977

[36] Romero J., Garcıa-Beltran A., and Hernandez-Andres J., 1997, *Linear bases for representation of natural and artificial illuminants*, J. Opt. Soc. Am. A 14, 1007–1014

[37] Hernandez-Andres J., Romero J. and Nieves J.L., 2001, *Color and spectral analysis of daylight in southern Europe*, Vol. 18, No. 6/June 2001/ J. Opt. Soc. Am. A

[38] Imai F.H., Rosen M.R. and Berns R.S. 2002, *Comparative Study of Metrics for Spectral Match Quality,* CGIV 2002: The First European Conference on Colour Graphics, Imaging, and Vision

[39] Viggiano, J A Stephen, *Metrics for evaluating spectral matches: a quantitative comparison*. Proceedings of CGIV-2004: the Second European Conference on Colour

Graphics, Imaging, and Vision. Springfield, VA: IS&T — The Society for Imaging Science & Technology, 2004, in press.

[40] Lopez-Alvarez M.A., Hernandez-Andres J., Valero E.M. and Nieves J.L., *Colorimetric and Spectral Combined Metric for the Optimization of Multispectral Systems* , AIC Colour 05 - 10th Congress of the International Colour Association

[41] Connah D., Hardeberg J. Y., 2004, *Comparison of linear spectral reconstruction methods for multispectral imaging*, Internation Conference of Image Processing (ICIP 2004)

[42] Xrite Color Checker Digital SG, [Online]. Available: http://xritephoto.com/ph_product_overview.aspx?id=938

[43] Specim Imspector V10E datasheet [Online]. Available: http://www.specim.fi/files/pdf/core/datasheets/VIS-VNIR-ImSpectors-ver1-2011.pdf

[44] Specim Imspector V10E photo. [Online]. Available: http://www.aelab.co.za/images/stories/specim/imaging_spectograph/vis_vnir/vnir/vnir1.jpg

[45] Shimano N., July 2006, *Recovery of Spectral Reflectances of Objects Being Imaged Without Prior Knowledge*, IEEE Transactions on Image Processing, Vol.15, No.7, July 2006

[46] Imai F. H., Berns R. S., 1999, *Spectral Estimation Using Trichromatic Digital Cameras*, Proceedings of the International Symposium on Multispectral Imaging and Color Reproduction for Digital Archives (Society of Multispectral Imaging of Japan, Chiba University, Japan, 1999)

[47] Komiya Y., Ohsawa K., Obi T., Yamaguchi M., Ohyama N., 1999, *Natural Color Reproduction System for Telemedicine and Its Application to Digigal Camera*, Proc IEEE, 50 54 (1999)

[48] Abrardo A., Alparone L., Cappellini V., Prosperi A., 1999, *Color Constancy fom Multispectral Images*, Proc. IEEE 570, 574 (1999)

[49] Hardeberg J. Y., 1999, *Acquisition and reproduction of colour images: colorimetric and multispectral approaches*, PhD Thesis (Ecole Nationale Superieure des Telecommunications, Departament TSI, Paris, France, 1999)

[50] Quijano Ruiz J. I, September 2010, *Quality metrics for spectral estimation,* Master thesis in Photonics, registered at Escola Tecnica Superior D'Enginyeria de Telecomunicacio de Barcelona.

[51] Wyszecki G, *Color Science: concepts and methods, quantitative data and formulae*, (John Wiley & Sons, New York, 1982).

[52] CIE Publication 142, *Improvement to Industrial Colour-Difference Evaluation,* Commission Internationale de L'Éclairage, (Vienna, Austria, 2001).

[53] Bayer E. B.,1 976, *Color imaging array,* U.S. Patent No. 3,971,065

[54] Antikainen J, 2012, *New Techniques for Spectral Image Acquisition and Analysis*, PhD thesis, Publications of the University of Eastern Finland Dissertations in Forestry and Natural Sciences, No 73

[55] Jetsu T., Hertzog P., Jaaskelainen T. and Parkkinen J., 2005, *Standardization of spectral Image Formats,* Pattern recognition and Image analysis, 15, 618-620

[56] Hauta-Kasari M., Lehtonen J., Parkkinen J., and Jääskeläinen T., *Image Format for Spectral Image Browsing*, IS & T Journal of Imaging Science and Technology 50 (2006).

[57] Swain P.K. Cheskis D., *Back-Illuminated Image Sensors Come to the Forefront* [Online], Available: http://www.photonics.com/Article.aspx?AID=34685

[58] *Sony develops back-illuminated CMOS image sensor* [Online], Available: http://www.sony.net/SonyInfo/News/Press/200806/08-069E/index.html

[59] *BSI (Backside Illumination)* [Online], Available: http://www.semicon.toshiba.co.jp/eng/product/sensor/cmos/bsi/index.html

[60] Cardinal D., *How back-illuminated sensors work, and why they're the future of digital photography* [Online], Available: http://www.extremetech.com/extreme/149742-how-back-illuminated-sensors-work-and-why-theyre-the-future-of-digital-photography

[61] *An Objective Look at FSI and BSI*, An AptinaTM Technology White Paper [Online], Available: http://www.aptina.com/news/FSI-BSI-WhitePaper.pdf

[62] *Spectral Image data cube* [Online], Available: http://zeiss.magnet.fsu.edu/tutorials/spectralimaging/lambdastack/lambdastacktutorialfigure1.jpg

[63] Peterson C., *How It Works: The Charged-Coupled Device, or CCD* [Online], Available: http://www.if.ufrgs.br/~marcia/ccd.pdf

[64] *Buried channel charge coupled devices*, US Patent US 3792322 A, [Online], Available: http://www.google.com./patents/US3792322

[65] Taylor S. A., *CCD and CMOS Imaging Array Technologies: Technology Review,* Technical Report EPC-1998-106, Xerox Research Centre Europe, 1998, [Online], Available: http://research.microsoft.com/pubs/80353/ccd.pdf

[66] Baker, R. J. (2010). *CMOS: Circuit Design, Layout, and Simulation*, Third Edition. Wiley-IEEE. p. 1174. ISBN 978-0-470-88132-3. http://CMOSedu.com

[67] Ohta N., Robertson A. R., 2005, *Colorimetry. Fundamentals and Applications,* published by John Wiley & Sons Ltd

[68] *Structure of human eye – photo*, [Online], Available http://www.odec.ca/projects/2005/dela5s0/public_html/structure.jpg

[69] Berns R. S., *Principle of Color Technology*, Wiley, USA, 2000

[70] Hunt R. W. G., 1988, *Measuring Color*, 3rd Edition, Ellis Harwood, Chichester, England.

[71] Absorption curves of cone cells in a typical human retina - photo , [Online], Available:
http://upload.wikimedia.org/wikipedia/commons/thumb/1/1e/Cones_SMJ2_E.svg/287px-Cones_SMJ2_E.svg.png

[72] Malacara D., Color *Vision and Colorimetric Theory and Applications,* SPIE, USA, 2002

[73] Sharma G., *Digital Color Imaging Hand Book*, CRC Press, New York , 2003

[74] Pennebaker W. B., Mitchell J. L., *JPEG – Still Image Data Compression Standard*, Eighth printing 2004 by Kluwer Academic Publishers

[75] Nokia Pureview Technology [Online], Available: http://www.nokia.com/global/innovation/pureview/

[76] Kerr D. A., *Chrominance Subsampling in Digital Images*, issue 3, January 19, 2012, [Online], Available: http://dougkerr.net/Pumpkin/articles/Subsampling.pdf

[77] Wallace G. K., 1991, *The JPEG Still Picture Compression Standard*, submitted for publication in IEEE Transactions on Consumer Electronics

[78] Dwivedi V., JPEG *Image Compression and Decompression with modeling of DCT coefficients on the Texas Instrument Video Processing Board TMS320DM6437*, master thesis in Electrical and Electronic Engineering, at California State University, Sacramento, 2010

[79] Lehtonen J. and Parkkinen Jussi, 2006, *Optimal sampling of color spectra*, Vol. 23, No. 12/December 2006/J. Opt. Soc. Am. A

[80] Bersha K. S., *Spectral Imaging and Analysis of Human Skin*, Master thesis report, 2010, University of Eastern Finland, Joensuu

[81] Hauta Kasari M., 1999, *Computational Techniques for Spectral Image Analysis*, PhD thesis, Lappeenranta Univeristy of Technology, Lappeenranta , Finland

[82] Penczek J., Boyton P. A. and Splett J.D., *Color Error in Digital Camera Image Capture Process*, J Digit Imaging (2014) 27:182–191

[83] Eriksson M. and Iqbal Z., *Two measurement modes for mobile phone optical sensing*, 2014, Sensors and actuators. B, Chemical, (195), 63-70. Available: http://dx.doi.org/10.1016/j.snb.2014.01.005

[84] Garcia A., Erenas M.M., Marinetto E. D., Abad C. A., de Orbe-Paya I., Palma A. J. and Capitan-Vallvey L. F., *Mobile Phone Platform as portable chemical analyzer*., Elsevier , Sensors and Actuators B 156 (2011) 350–359

[85] Iqbal Z., Bjorklund R.B., *Assesment of a mobile phone for use as a spectroscopic analytical tool for foods and beverages*, International Journal of Food Science and Technology 2011, 46, 2428–2436

[86] Iqbal Z., Filippini D., *Spectral Fingerprinting on a Standard Mobile Phone* , Hindawi Publishing Corporation, Journal of Sensors, Volume 2010, Article ID 381796, 9 pages doi:10.1155/2010/381796

[87] Alakarhu J., Image *Sensors and Image Quality in Mobile Phones*, Nokia, Technology Platforms, Camera Entity

ANNEX A

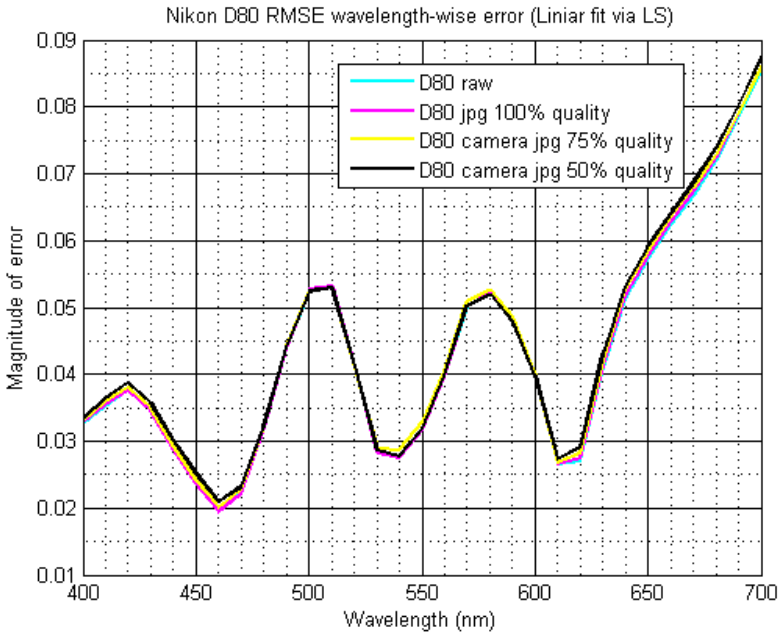

Figure 33 RMSE wavelength-wise error (Liniar fit via LS) for Nikon D80 in testing the influence of JPEG compression in reflectance estimation (spatial homogenous case)

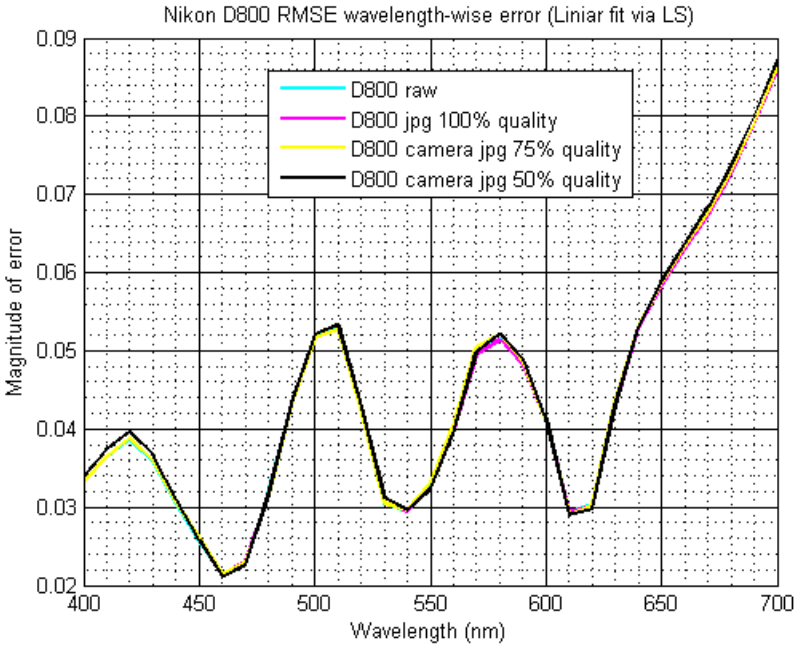

Figure 34 RMSE wavelength-wise error (Liniar fit via LS) for Nikon D800 in testing the influence of JPEG compression in reflectance estimation (spatial homogenous case)

Table 21 CIELAB and CIEDE2000 color difference (Liniar fit via LS) for Nikon D800 in testing the influence of JPEG compression in reflectance estimation (spatial homogenous case)

	CIELAB				CIEDE2000			
	Min	Mean	Max	Standard deviation	Min	Mean	Max	Standard deviation
D80raw	0.5	3.7	11.0	2.3	0.3	2.4	7.9	1.3
D80 JPEG 100%	0.3	3.7	11.3	2.3	0.5	2.4	8.3	1.3
D80 JPEG 75%	0.5	4.3	12.7	2.6	0.4	2.7	8.9	1.6
D80 JPEG 50%	0.7	4.1	14.0	2.9	0.6	2.5	12.5	1.5
D800raw	0.3	3.9	12.5	2.5	0.4	2.5	8.7	1.4
D800JPEG 100%	0.5	4.1	13.3	2.6	0.6	2.6	8.9	1.6
D800 JPEG 75%	0.8	4.4	13.0	2.8	0.5	2.9	11.6	2.0
D800 JPEG 50%	0.7	4.9	23.5	3.8	0.4	3.1	16.3	2.7

Table 22 RMSE and GFC errors (Liniar fit via LS) for Nikon D800 in testing the influence of JPEG compression in reflectance estimation (spatial homogenous case)

	RMSE				GFC			
	Min	Mean	Max	Standard deviation	Min	Mean	Max	Standard deviation
D80 raw	0.014	0.042	0.115	0.018	0.786	0.977	0.999	0.036
D80 JPEG 100%	0.013	0.042	0.117	0.018	0.781	0.977	0.999	0.037
D80 JPEG 75%	0.014	0.042	0.120	0.019	0.792	0.977	0.999	0.037
D80 JPEG 50%	0.015	0.043	0.114	0.018	0.768	0.976	0.999	0.039

D800 raw	0.014	0.043	0.114	0.018	0.798	0.978	0.999	0.035
D800 JPEG 100%	0.013	0.043	0.114	0.018	0.799	0.978	0.999	0.034
D800 JPEG 75%	0.015	0.043	0.113	0.018	0.796	0.978	0.999	0.035
D800 JPEG 50%	0.008	0.043	0.119	0.019	0.799	0.977	0.999	0.035

ANNEX B

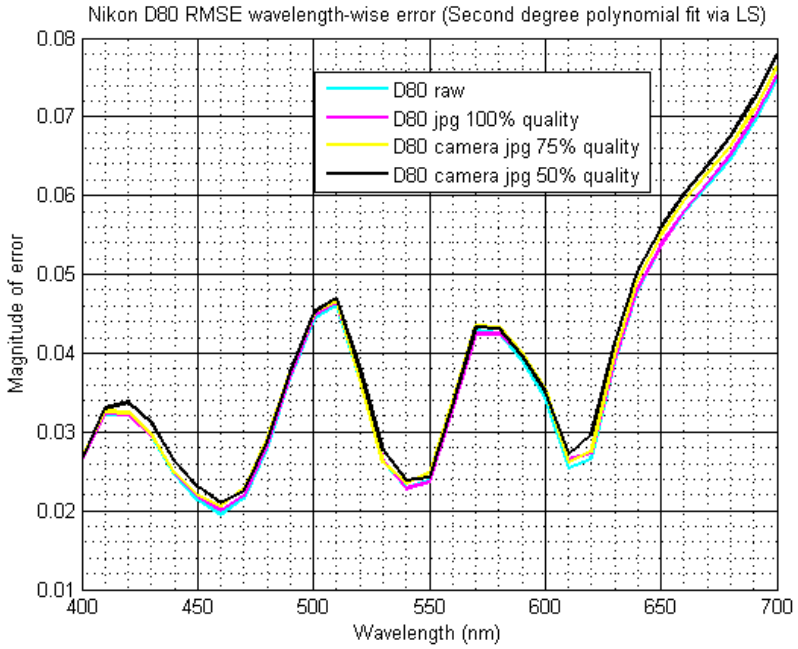

Figure 35 RMSE wavelength-wise error (Second degree polynomial fit via LS) for Nikon D80in testing the influence of JPEG compression in reflectance estimation (spatial homogenous case)

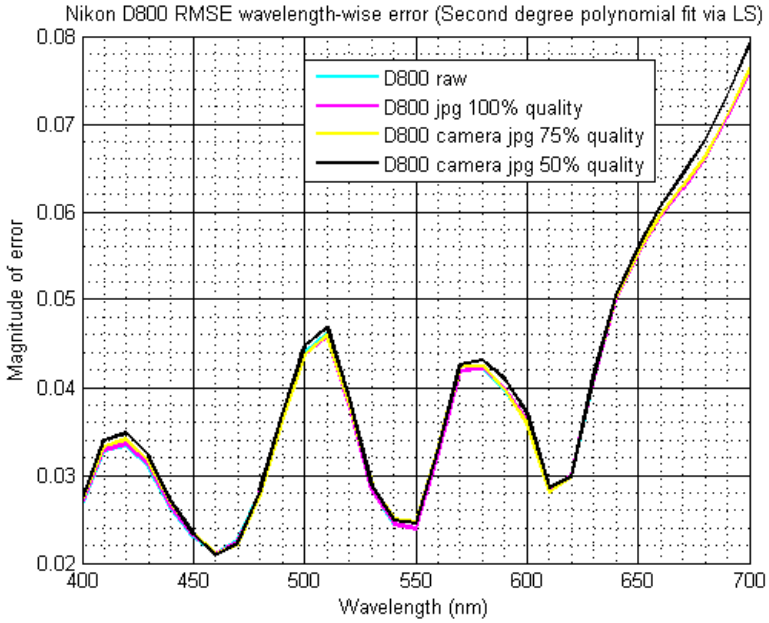

Figure 36 RMSE wavelength-wise error (Second degree polynomial fit via LS) for Nikon D800 in testing the influence of JPEG compression in reflectance estimation (spatial homogenous case)

Table 23 CIELAB and CIEDE2000 color difference (Second degree polynomial fit via LS) for Nikon D80 in testing the influence of JPEG compression in reflectance estimation (spatial homogenous case)

	CIELAB				CIEDE2000			
	Min	Mean	Max	Standard deviation	Min	Mean	Max	Standard deviation
D80 raw	0.2	2.8	8.1	1.7	0.2	1.7	4.1	0.8
D80 JPEG 100%	0.5	2.9	8.6	1.7	0.3	1.8	5.1	0.9
D80 JPEG 75%	0.4	3.4	15.6	2.6	0.3	2.0	6.1	1.2
D80 JPEG 50%	0.3	3.9	15.3	2.8	0.2	2.3	10.31	1.6
D800 raw	0.7	2.8	10.5	1.8	0.5	1.7	4.7	0.8
D800JPEG 100%	0.6	3.1	10.0	1.9	0.3	1.9	4.7	0.9
D800 JPEG 75%	0.5	3.6	13.0	2.3	0.4	2.3	10.1	1.5
D800 JPEG 50%	0.3	4.1	20.6	3.1	0.2	2.4	14.9	2.0

Table 24 RMSE and GFC errors (Second degree polynomial fit via LS) for Nikon D80 in testing the influence of JPEG compression in reflectance estimation (spatial homogenous case)

	RMSE				GFC			
	Min	Mean	Max	Standard deviation	Min	Mean	Max	Standard deviation
D80 raw	0.007	0.037	0.083	0.016	0.816	0.984	0.999	0.027
D80 JPEG 100%	0.008	0.037	0.085	0.016	0.793	0.984	0.999	0.029
D80 JPEG 75%	0.011	0.038	0.093	0.017	0.795	0.983	0.999	0.029
D80 JPEG 50%	0.011	0.039	0.085	0.016	0.787	0.983	0.999	0.030

D800 raw	0.007	0.038	0.083	0.017	0.816	0.984	0.999	0.026
D800 JPEG 100%	0.008	0.038	0.083	0.017	0.807	0.984	0.999	0.027
D800 JPEG 75%	0.007	0.038	0.081	0.017	0.819	0.985	0.999	0.026
D800 JPEG 50%	0.009	0.038	0.089	0.018	0.798	0.983	0.999	0.030